AER/AGS Special Report 117

Alberta Energy Regulator

Deep Electrical Structure of the Buffalo Head Hills and Birch Mountains, Northern Alberta: Implications for Diamond Exploration

AGS
ALBERTA GEOLOGICAL SURVEY

AER/AGS Special Report 117

Deep Electrical Structure of the Buffalo Head Hills and Birch Mountains, Northern Alberta: Implications for Diamond Exploration

B.F.W. Chase[1], M.J. Unsworth[1], D.I. Pană[2] and E. Wang[1]

[1] Department of Physics, University of Alberta
[2] Alberta Energy Regulator
Alberta Geological Survey

March 2024

ISBN 978-1-4601-5717-6

Chase, B.F.W., Unsworth, M.J., Pană, D.I. and Wang, E. (2024): Deep electrical structure of the Buffalo Head Hills and Birch Mountains, northern Alberta: implications for diamond exploration; Alberta Energy Regulator / Alberta Geological Survey, AER/AGS Special Report 117, 40 p.

Publications in this series have undergone only limited review and are released essentially as submitted by the author.

Authors address:
B.F.W. Chase, M.J. Unsworth and E. Wang
Department of Physics
University of Alberta
Edmonton, AB T6G 2E3
Canada

Tel: 780.492.3041
Email: bchase1@ualberta.ca

Published March 2024 by:
Alberta Energy Regulator
Alberta Geological Survey
Suite 205
4999 – 98 Avenue NW
Edmonton, AB T6B 2X3
Canada

Tel: 780.638.4491
Email: AGS-Info@aer.ca
Website: ags.aer.ca

Contents

Figures

Acknowledgements

The authors are grateful to Zoë Vestrum, Erich Slobodian, Cedar Hanneson, and Javier Gonzalez (University of Alberta) for their assistance with data collection. Alberta Energy Regulator personnel who helped with permitting are also thanked. The three-dimensional magnetotelluric inversions used ModEM: the Modular system for Electromagnetic inversion supplied by Anna Kelbert. The Digital Research Alliance of Canada is thanked for use of their computer resources to run inversions. Maps were prepared using The Mathworks, Inc.'s MATLAB and Esri's ArcGIS®.

Abstract

Geophysical studies on several continents have shown that diamondiferous kimberlites are sometimes spatially associated with geophysical anomalies in the lithospheric mantle. This includes magnetotelluric (MT) studies that have shown that diamondiferous kimberlites are sometimes underlain by zones of low electrical resistivity (conductors) in the lithosphere. A number of explanations have been proposed for the low resistivity of these regions and include (1) lithosphere enrichment, (2) the formation of hydrous minerals by metasomatism, or (3) the presence of conductive mineral phases such as graphite and sulphides. The relationship between these low resistivity anomalies and kimberlite diamond potential has been suggested as having value in exploration. However, this link has not been definitively established. Northern Alberta is an ideal location to further evaluate this relationship because the region hosts two distinct kimberlite fields, the Buffalo Head Hills and Birch Mountains fields. These kimberlite fields are underlain by regions of the mantle with different values of electrical resistivity. The Buffalo Head Hills kimberlite field has good diamond potential and is underlain by a resistive lithospheric mantle. The Birch Mountains kimberlite field has poor diamond potential and is underlain by a major lithospheric mantle conductor. The study of the kimberlites and the surrounding regions has produced xenolith analytical, mantle petrological, and regional geophysical data that can be integrated with the MT data in order to provide a more rigorous interpretation of the properties of the lithosphere. Ultimately, the spatial relationship between lithospheric mantle conductors and diamondiferous kimberlites may be a useful tool in area selection during diamond exploration.

The number of MT stations previously deployed in northern Alberta was quite limited, and parts of the resulting resistivity model were poorly resolved. To improve model resolution, the University of Alberta and the Alberta Energy Regulator undertook a long-period MT survey in northern Alberta in the summer and fall of 2022. In total 15 stations were deployed and spaced approximately every 50 km. The survey was aimed at filling in a gap in MT station coverage between the two kimberlite fields as well as placing additional MT stations above the conductor beneath the Birch Mountains kimberlite field. Time-series data were acquired and used to compute apparent resistivity and phase data in the period range of 1–10 000 seconds. Three-dimensional (3D) MT inversion was used to convert these MT data into an electrical resistivity model of the region that imaged the entire lithosphere. The 3D resistivity model shows that the conductor beneath the Birch Mountains kimberlite field does not extend west towards the Buffalo Head Hills kimberlite field, and that it is narrower than previously imaged. The new MT data also help to remove uncertainty about the spatial position and geometry of this conductor, which was previously constrained by data from only a few MT stations. Initial modelling results suggest that the prior interpretations of the conductor being caused by lithosphere enrichment or hydrous minerals is valid. A more extensive mantle resistivity modelling approach will be undertaken in the future to fully evaluate which conductivity-enhancing mechanism can best explain the low resistivity observed beneath the Birch Mountains kimberlite field. These results will be integrated with regional xenolith analytical, mantle petrological, and geophysical data to determine if there is a genetic relationship between the low resistivity anomaly and kimberlite diamond potential.

This work was completed under the Mineral Grant provided by the Government of Alberta dated June 22, 2021.

1 Introduction

Diamonds are formed in the deep lithospheric mantle where the pressure is high enough to allow carbon to turn into diamond. Diamonds are brought to the surface by the eruptions of kimberlites, which are small volume, volatile-rich melts that originate in the asthenosphere. As kimberlites ascend through the lithospheric mantle to the Earth's surface they entrain xenoliths, which can include diamonds if they are present (Russell et al., 2019). Although originally associated with Archean lithosphere, kimberlites and diamonds have recently been shown to frequently form and erupt within Proterozoic terranes (e.g., Liu et al., 2018; Czas et al., 2020). This has expanded the search area for kimberlite pipes that may contain economically significant quantities of diamonds. Kimberlite exploration is inherently challenging because pipes are usually less than 1 km in diameter and typical exploration areas are hundreds to thousands of kilometres in extent. As diamond exploration in Canada moves towards greenfield areas (i.e., unexplored regions) alongside more difficult targets in brownfields (i.e., previously developed or explored regions), additional criteria will be invaluable for area selection to help lower exploration costs.

Magnetotelluric (MT) data have been used to study the electrical resistivity structure of the lithosphere in regions containing diamondiferous kimberlites including in the Northwest Territories, Saskatchewan, and South Africa (e.g., Özaydın and Selway, 2022; Bettac et al., 2023). The interpretation of these MT data has proven useful for kimberlite exploration in two ways: (1) detecting upper mantle resistivity anomalies that may be correlated with diamondiferous kimberlites, and (2) providing information about the depth to the lithosphere-asthenosphere boundary (LAB).

Regarding the detection of anomalies, studies in a number of cratons have shown that diamondiferous kimberlites pipes are sometimes spatially associated with regions of low electrical resistivity (high conductivity) in the lithospheric mantle (e.g., Jones et al., 2005; Özaydın and Selway, 2022; Wang and Unsworth, 2022; Bettac et al., 2023). In particular, Özaydın and Selway (2022) showed that in various cratons kimberlites tend to be distributed along the margins of conductors and avoid the most resistive and most conductive regions. An early interpretation was that these conductors represented carbon in the form of graphite, which was identified as the carbon that led to diamond growth (e.g., Jones et al., 2005; Türkoğlu et al., 2009). Geochemical data and laboratory experiments have cast doubt on these interpretations, noting that graphite films are only stable at crustal depths and may be a transient feature, potentially lasting for only a few tens of thousands of years (Zhang and Yoshino, 2017). Additionally, the mantle is generally too oxidizing for graphite film formation, even at shallow depths, with the carbon producing carbonate minerals rather than graphite (Frost and McCammon, 2008). More recent interpretations have suggested that the low resistivity is due to metasomatism, a process where the lithosphere is modified by fluids. These studies have concluded that a degree of fluid or melt metasomatism is necessary to produce diamondiferous kimberlites (e.g., Özaydın and Selway, 2022), an interpretation that is consistent with geochemical results (Stachel and Luth, 2015).

The nature of this metasomatism and its genetic relationship with lithospheric mantle conductors and the diamond potential of kimberlites remains unclear. Northern Alberta is an excellent region to investigate this relationship. The region hosts two distinct kimberlite clusters known as the Birch Mountains and Buffalo Head Hills kimberlite fields (Figure 1). Of the two, the Buffalo Head Hills kimberlite field has the best diamond potential, including the possibility that large ultradeep diamond sources exist in the asthenosphere (Banas et al., 2007; Eccles, 2011). In comparison, the Birch Mountains kimberlite field appears to have poor diamond potential (Eccles, 2011). Interestingly, the Birch Mountains kimberlite field is underlain by a low resistivity anomaly in the lithospheric upper mantle. In contrast, the Buffalo Head Hills kimberlite field is not underlain by a conductor (Wang and Unsworth, 2022). The conduction mechanisms and tectonic processes responsible for these contrasting mantle resistivity anomalies remains unclear, as does the relationship between the geophysical anomalies and the diamond potential of each kimberlite field.

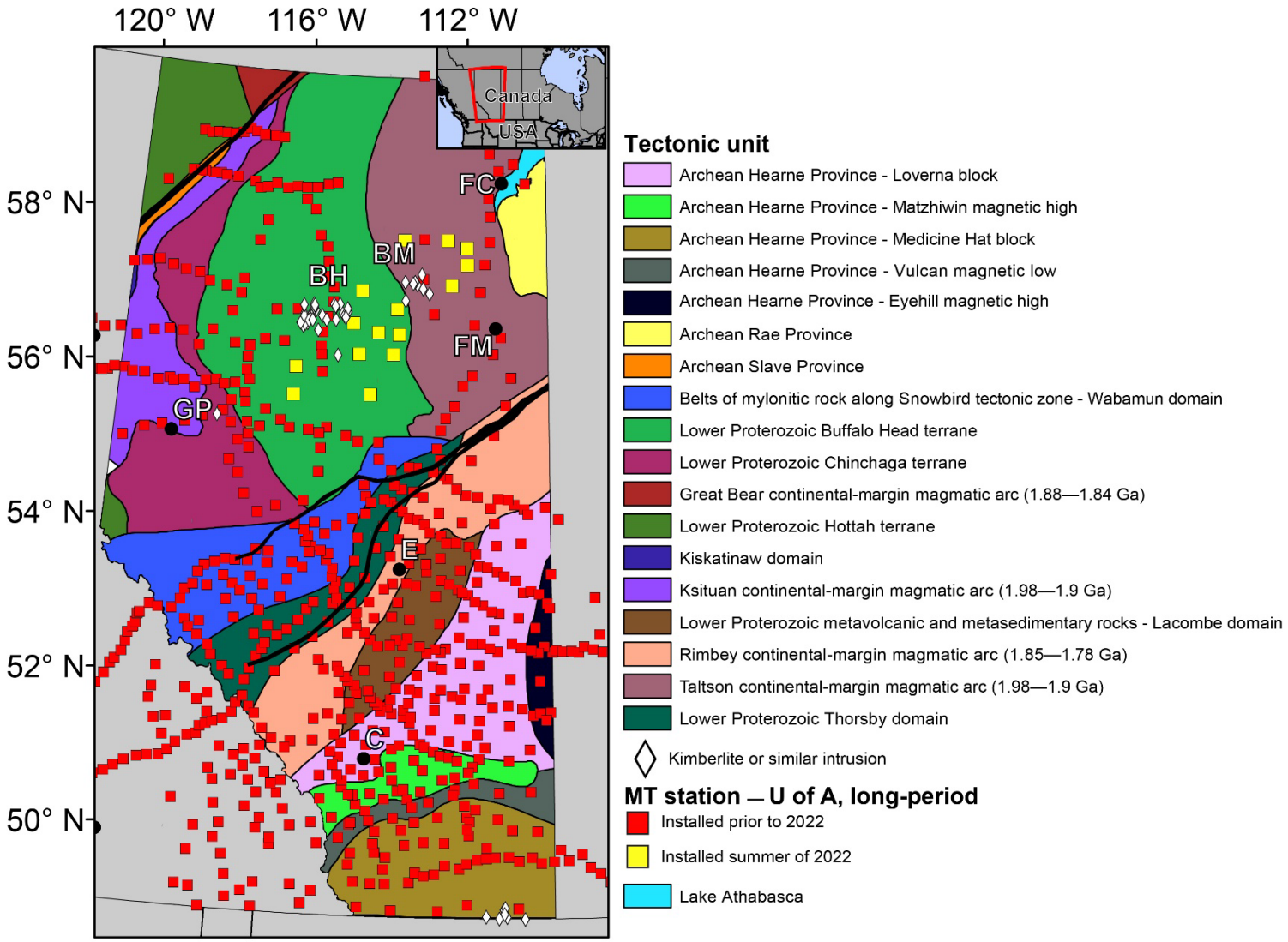

Figure 1. Tectonic map of Alberta showing sites of the University of Alberta's (U of A) long-period magnetotelluric (MT) stations that collected data for this study. Sites shown with yellow symbols are those stations deployed in 2022 with Alberta Energy Regulator support. Thick black lines represent major shear zone boundaries and faults. Abbreviations: BH, Buffalo Head Hills kimberlite field; BM, Birch Mountains kimberlite field; C, Calgary; E, Edmonton; FC, Fort Chipewyan; FM, Fort McMurray; GP, Grand Prairie.

Carbon is only stable in the form of diamond in the lower lithosphere at pressures greater than 3–5 GPa. This provides an upper limit on the depths at which diamonds can be formed. In settings with a colder geotherm, the diamond stability window begins at a shallower depth and has a greater depth extent. This may permit ascending kimberlites to encounter and entrain more diamonds, producing a greater diamond potential at the surface. The lower depth limit on diamond stability in the lithosphere is the depth of the LAB. Identification of minerals entrained by kimberlites can be used to produce geotherms useful for estimating the vertical extent of the diamond stability window. However, the depth distribution of these minerals is often nonuniform. An alternative approach uses geophysical data to estimate the depth of the LAB. As MT and seismic data are often sensitive to the change in rock properties at the LAB, they can be used to independently estimate LAB depths over large areas (Eaton et al., 2009; Wang and Unsworth, 2022). This allows the depth extent of the diamond stability window to be determined in regions of interest. This can help to overcome limitations posed by kimberlites, which provide information over only a small area of the lithosphere or may not be accessible in certain exploration scenarios.

Continued development of the spatial and genetic relationship between lithospheric mantle conductors and diamondiferous kimberlites may have profound implications for diamond exploration. These deep mantle conductors could present much larger targets, useful for determining search areas during exploration. This, in combination with the ability of MT to image the LAB, makes MT a valuable reconnaissance tool when selecting target areas for exploration using more expensive techniques. In this report, new MT data collected in 2022 in the area around the Buffalo Head Hills and Birch Mountains kimberlite fields are discussed. These MT data were collected to improve upon the initial model of mantle resistivity structure in the region by Wang and Unsworth (2022). These new MT data will be used to determine (a) which conduction mechanisms caused the low resistivity zone detected in the mantle, (b) how these zones are related to regional tectonics, and (c) how the zones may be related to kimberlite diamond potential.

2 Geological Setting

The surficial geology in the region is characterized by glacial deposits and a 1–2 km thick section of Phanerozoic sedimentary rocks of the Western Canada Sedimentary Basin (WCSB). The kimberlites have intruded into these sedimentary rocks and reached the near surface. Beneath the WCSB, the rocks consist of crystalline basement terranes that were accreted to the continent during the assembly of Laurentia in the Paleoproterozoic (Hoffman, 1988). These basement terranes will be discussed separately in relation to each kimberlite field.

2.1 Buffalo Head Hills Kimberlite Field

The Buffalo Head Hills kimberlite field is located in the Buffalo Head terrane (Figure 1). This Paleoproterozoic terrane has an age of 2.3–2.0 Ga (Ross et al., 1994) and is interpreted to be a rifted sliver or accretionary terrane that first collided with the western Chinchaga domain during the collision of the Rae and Slave cratons (Ross, 2002). During accretion, it was located between west- and east-dipping subduction zones to the west and east, respectively (Ross, 2002; Ross and Eaton, 2002). An alternative model suggests that the west-dipping subduction zone was east dipping (Chaco et al., 2000). Another alternative model proposed that the basement is composed of Archean crustal materials that were reworked during the Paleoproterozoic (Burwash et al., 2000). This model does not appear to apply to the lithospheric mantle, as a lack of subcalcic G10 peridotitic garnets argues against the presence of Archean lithosphere (Eccles, 2011).

Kimberlite magmatism occurred in the Buffalo Head Hills kimberlite field during the Late Cretaceous to Paleocene, from ca. 88 to 60 Ma (Kravchinsky et al., 2009; Eccles, 2011). The kimberlite magma sampled a depleted lithosphere during ascent (Eccles and Simonetti, 2008). In total 41 kimberlite pipes have been mapped in the Buffalo Head Hills kimberlite field. Of these, 28 are diamondiferous and the highest

diamond grade was estimated at 55 carats per hundred tonnes (Eccles, 2011). The most economically attractive prospects are located in the northwestern portion of the field.

2.2 Birch Mountains Kimberlite Field

The Birch Mountains kimberlite field is located in the Taltson magmatic-arc terrane (or Taltson–Thelon orogenic belt; Figure 1). The Taltson terrane was formed in the Proterozoic as either a plate-margin magmatic arc over a west-dipping subduction zone (Ross, 2002) or a hinterland where magmatism was triggered in response to crustal thickening from far-field convergence farther west (Chacko et al., 2000). Both of these models suggest that the Taltson terrane was formed during the assembly of Laurentia, but differ in the location of the terrane with respect to the plate boundary and the presence of subduction in the region.

Kimberlite magmatism occurred in the Birch Mountains kimberlite field during the Late Cretaceous, from ca. 78 to 70 Ma (Eccles, 2011). In comparison to the Buffalo Head Hills kimberlite field, the kimberlite magma sampled either remarkably thin lithosphere or an extensively re-enriched asthenosphere-type mantle (Eccles, 2011). A few of the intrusions appear to have sampled or originated in shallow levels of the mantle compared to other regional kimberlites (Eccles, 2011). Of the eight known kimberlite bodies in the Birch Mountains kimberlite field, two do not fit the definition of kimberlites and instead appear similar to young (ca. 60 Ma) alkaline-ultrabasic intrusions in the Buffalo Head Hills kimberlite field (Eccles, 2011). Multiple kimberlites have been sampled for diamonds and have yielded diamond-poor scenarios with only a few micro- and macrodiamonds recovered (Eccles, 2011).

3 Previous Geophysical Surveys

Much of the geophysical data collected in northern Alberta remains in the private domain as part of hydrocarbon or mineral exploration and development efforts by industry. Publicly available data is limited and consists of gravity and aeromagnetic survey data of various vintages. Aeromagnetic data have been used extensively in diamond exploration. This is because the majority of kimberlites have a strong magnetic contrast with the surrounding sedimentary rocks (e.g., Pilkington et al., 2000; Ross and Eaton, 2002; Skelton et al., 2003). In cases where kimberlites are nonmagnetic, other geophysical methods are used in exploration. This includes electromagnetic, gravity, and seismic methods, which have helped to discover additional targets (Skelton et al., 2003). Investigations using aeromagnetic data to delineate regional deep-seated structures that controlled kimberlite emplacement have not yet been performed. However, seismic and gravity data have delineated the Peace River Arch, an east-northeast–trending basement-rooted structure that may have influenced kimberlite emplacement (Eccles, 2011).

Geophysical imaging at crustal and lithospheric mantle depths in the region has been performed using both MT and seismic data. The first major MT dataset was collected as part of the LITHOPROBE project in the 1990s. During LITHOPROBE, data were collected at 323 long-period MT stations in Alberta with the aim of studying the Paleoproterozoic basement terranes. This project included a number of MT stations near the Buffalo Head Hills kimberlite field. These data showed a one-dimensional (1D) resistivity structure in the upper 2–3 km that corresponded to the strata of the Western Canada Sedimentary Basin. The MT data also showed the presence of a two-dimensional (2D) resistivity structure at greater depths in the crystalline basement. A major crustal conductor, the Kiskatinaw conductor, was imaged near the Alberta–British Columbia border (Boerner et al., 2000).

For the past two decades, the University of Alberta has collected MT data at locations across the province with stations located near both the Buffalo Head Hills and Birch Mountains kimberlite fields (Figure 1). The depth of investigation depends on the type of instrument used and the length of recording. For upper crustal studies, broadband MT data is collected for 18–24 hours and produces data in the frequency band of 1000–0.001 Hz. For studies of the lower crust and upper mantle, lower frequencies (longer periods) are needed. Long-period MT data typically requires recording for 2–3 weeks at each location and produces data in the frequency range 1–0.0001 Hz, which corresponds to periods of 1 to 10 000 seconds. Long-

period MT data collected near the Buffalo Head Hills kimberlite field by Türkoğlu et al. (2009) showed additional conductors were spatially associated with terrane boundaries. The conductors were interpreted as zones where graphite films or sulphide minerals had been deposited by fluid movement during tectonism (Türkoğlu et al., 2009; Wang and Unsworth, 2022). The occurrence of graphite was significant because at upper mantle depths it could represent the carbon that resulted in diamond growth at greater depths (Türkoğlu et al., 2009). Wang et al. (2018) and Wang and Unsworth (2022) collected additional long-period MT data in the region and found additional conductors that they associated with terrane boundaries and faults. A recently published 3D resistivity model of the entire province produced by Wang and Unsworth (2022) shows that the lithospheric mantle is highly conductive beneath the Birch Mountains kimberlite field and highly resistive beneath the Buffalo Head Hills kimberlite field. The authors interpreted this difference to reflect more intense mantle enrichment and metasomatism beneath the Birch Mountains kimberlite field. This is in agreement with interpretations from regional seismic studies showing a low velocity seismic anomaly in the lithosphere beneath and around the Birch Mountains kimberlite field (Chen et al., 2020). The provincial MT dataset has also been used to interpret conductors related to the tectonic assembly of Alberta farther south (e.g., Nieuwenhuis et al., 2014) and for resource potential in specific areas (e.g., Liddell et al., 2016).

The study by Wang and Unsworth (2022) showed that additional long-period MT data collection was necessary near the kimberlite fields to improve resolution of upper mantle resistivity structure. Critically, the conductor beneath the Birch Mountains kimberlite field was constrained by only three MT stations, limiting the resolution of its geometry. Additionally, no MT data were available from the region between the two kimberlite fields. As a result, the spatial relationship between the conductor beneath the Birch Mountains kimberlite field and region beneath the Buffalo Head Hills kimberlite field was unclear. The current study focused on collecting additional MT data in order to overcome these limitations of the previous work.

4 Magnetotelluric Data Collection in 2022

The MT survey was planned by the University of Alberta and Alberta Energy Regulator for 2022 in order to improve MT station coverage and address the concerns described above. The survey was conducted in two phases. The first phase aimed to collect MT data between the Birch Mountains and Buffalo Head Hills kimberlite fields where no long-period MT data had been previously collected. This phase aimed at determining if any conductors were present in the lithosphere between the two kimberlite fields or if the conductor beneath the Birch Mountains kimberlite field extended farther west. The second phase aimed to collect additional data around the Birch Mountains kimberlite field in order to improve the resolution of the Birch Mountains conductor (BMC; Wang and Unsworth, 2022), which was previously constrained by data from only a few MT stations (Figure 1). Long-period MT data were collected because they can be used for imaging to the base of the lithosphere.

Over the two phases, 15 long-period MT stations were deployed with an interstation spacing of approximately 50 km (Figure 1). At each location, the MT stations recorded data for 10–14 days. The MT data were recorded with Narod Geophysics Ltd.'s NIMS (Narod Intelligent Magnetotelluric System) long-period MT instruments, which are owned and operated by the University of Alberta. These MT instruments record two orthogonal electric field components and three magnetic field components as a function of time (Figure 2) with an 8 Hz sampling rate. Following best practices for data collection, electrodes were buried 30–40 cm below the surface to avoid the effects of daily temperature variations and precipitation. Bentonite was placed in the electrode holes to improve electrical contact with the ground. Each station was time synchronized using GPS in order to allow for the comparison of the time series and noise removal. Despite extensive oil and gas production infrastructure in the region, cultural noise was minimal, and the MT stations were always installed more than 500 m away from any major infrastructure. Each station produced approximately 150 MB of time-series data.

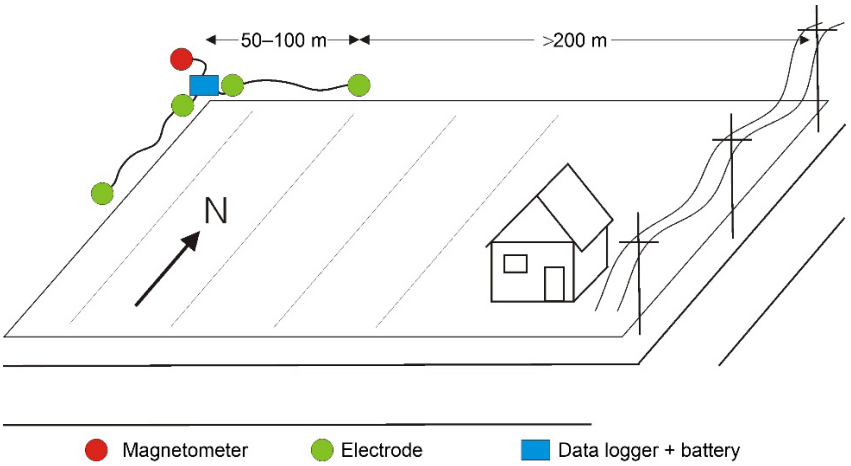

Figure 2. Schematic cartoon showing the layout of a typical magnetotelluric (MT) site. Note that components are not to scale.

5 Magnetotelluric Data Analysis

The MT method uses natural electromagnetic signals that penetrate the Earth to measure subsurface resistivity. At frequencies greater than 10 Hz, these signals are generated by global lightning activity, and below 1 Hz they are primarily generated by interactions between solar wind and the magnetosphere (Simpson and Bahr, 2005). The depth of signal penetration is proportional to the period (T; the reciprocal of frequency) of the signal and is represented by

$$\delta = 503\sqrt{\rho T}\,, \tag{1}$$

where ρ is the electrical resistivity of the Earth measured in ohm•metres (Ω•m) and δ is the depth of signal penetration, called the skin depth, measured in metres. Figure 3 shows how the skin depth, as a function of period, decreases in mediums with lower electrical resistivity values. Typically, signals recorded by long-period MT systems are capable of imaging the entire lithosphere.

5.1 Time-Series Analysis

The electric and magnetic field data are recorded in the time domain. They are then transformed into the frequency domain using Fourier analysis to give spectra as a function of frequency. The magnetic field spectra are $H_x(\omega)$, $H_y(\omega)$, and $H_z(\omega)$ and the electric field spectra are $E_x(\omega)$ and $E_y(\omega)$, where ω is the angular frequency. These quantities can be related by

$$Z_{ij} = \frac{E_i(\omega)}{H_j(\omega)}\,, \tag{2}$$

where Z is the impedance tensor, and i and j are the x, y, or z components of the respective orthogonal fields. For 3D analysis and modelling, the MT impedance is a complex-valued, full-rank, second-order tensor represented by

$$Z(\omega) = \begin{bmatrix} Z_{xx}(\omega)\; Z_{xy}\;(\omega) \\ Z_{yx}(\omega)\; Z_{yy}(\omega) \end{bmatrix}. \tag{3}$$

Apparent electrical resistivity can be obtained from the impedance by

$$\rho_{ij}(T) = \frac{T}{2\pi\mu}\left|Z_{ij}\right|^2\,, \tag{4}$$

where μ is the magnetic permeability of free space. The apparent resistivity provides an estimate of the electrical properties of the subsurface. Regions of low resistivity can indicate the presence of water, melt, lithosphere modification, and hydrous mineral phases, which can be related to tectonic processes.

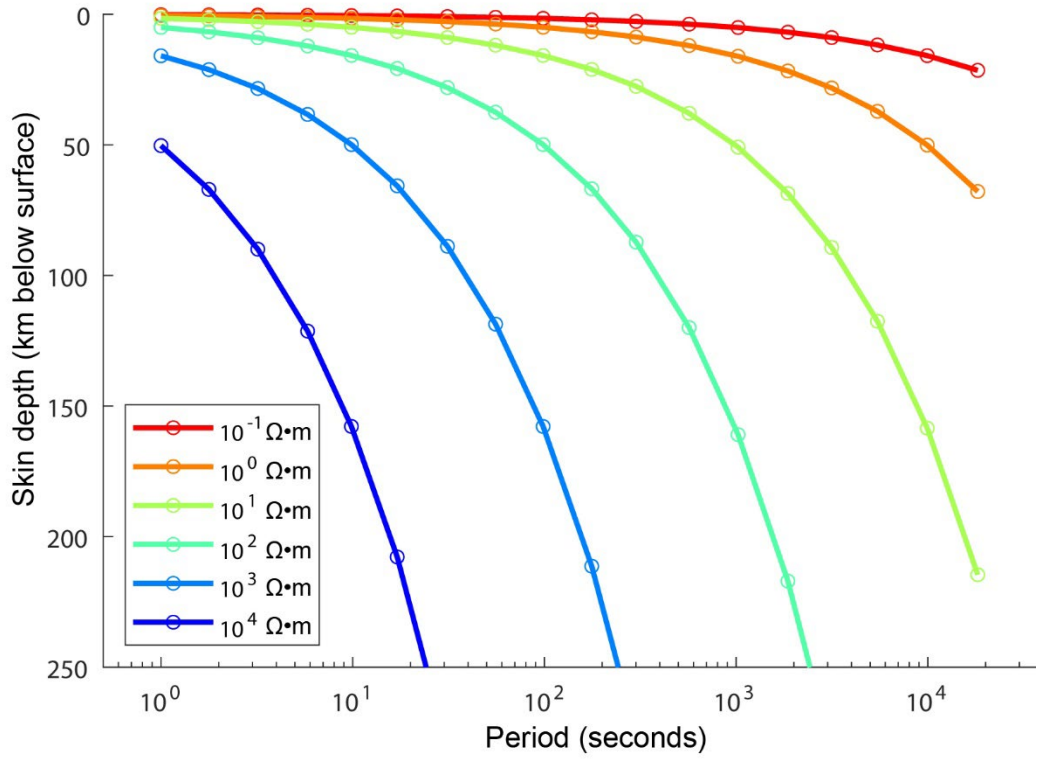

Figure 3. Illustration of the skin depth concept. At higher resistivity values (on the left), the lowest frequency signals penetrate deeper than 250 km. At lower resistivity values (on the right), the lowest frequency signals are quickly attenuated within the upper 50 km of the lithosphere. Figure modified from Hanneson and Unsworth (2023). Abbreviation: Ω, ohm.

5.2 Apparent Resistivity, Phase, and Tipper Curves

The apparent resistivity, phase, and tipper curves for each new site are shown in Appendix 1 (Figures 14–28). In these figures, the red and blue curves in the apparent resistivity window correspond to the XY and YX components of the data, respectively. The XY component is computed from the north-south electric field and east-west magnetic field. The YX component is computed from the east-west electric field and the north-south magnetic field. If the two curves are coincident, this can indicate that the subsurface is characterized by a 1D resistivity structure. Differences between the curves can indicate the presence of a 2D or 3D resistivity structure. Determination of dimensionality requires that the apparent resistivity and phase are examined as a function of a coordinate system.

A common pattern in the northern Alberta data is that as period increases, the apparent resistivity rises then falls. This generally reflects a three-layer resistivity structure with

1) a near-surface, low resistivity layer that can be identified as the sedimentary rocks of the WCSB,
2) an underlying high resistivity layer that can be identified as the lithosphere, and
3) a deep, low resistivity layer that can be identified as the asthenosphere.

There are some systematic differences between the 15 sounding curves (Figures 14–28), generally in the degree to which the XY and YX data components are different at periods greater than 10–100 seconds. This indicates deviations from a simple 1D resistivity model. To determine a resistivity model, a formal inversion process is required, as described below (Section 6).

5.3 Phase Tensors

The dimensionality of the MT data was evaluated using phase tensors. Phase tensors display the azimuthal variation of the impedance and give a graphical way, in the form of a coloured circle or ellipse, to determine if the subsurface has a 1D, 2D, or 3D resistivity structure (Caldwell et al., 2004). The direction of the major axis (i.e., long axis) of the ellipse is either parallel or perpendicular to the geoelectric strike, typically representing the conductive anomalies of interest. A parameter called the skew angle is also calculated, it indicates the dimensionality and is represented by the colour of the circle (Booker, 2014). A circular phase tensor with zero skew reflects a 1D resistivity structure, an elliptical tensor with zero skew indicates a 2D resistivity structure, and an elliptical tensor with non-zero skew indicates a 3D resistivity structure (Caldwell et al., 2004; Booker, 2014). An important aspect of the phase tensor is that it is not affected by near-surface galvanic distortions (Booker, 2014).

The phase tensors in Alberta are shown in Figure 4. At periods of less than 20 seconds, the data are 3D in nature, which reflects the low resistivity and structural complexity of the WCSB. For periods from 20 to 200 seconds, the data are again 3D in nature around the Birch Mountains kimberlite field, which corresponds to the BMC noted by Wang and Unsworth (2022). Around the Buffalo Head Hills kimberlite field, the 3D dimensionality likely reflects a conductive structure east of the kimberlite field, as observed by Türkoğlu et al. (2009), Wang et al. (2018), and Wang and Unsworth (2022). In the period range of 200–2000 seconds, the dimensionality of the data becomes more 1D to 2D, likely reflecting a simpler lithosphere structure below the major conductors. At periods greater than 2000 seconds, the data again become 3D, likely reflecting the complexity of the asthenosphere and LAB in the region (Wang and Unsworth, 2022).

6 3D Inversion of Magnetotelluric Data

The MT data presented in Figures 4 and 14–28 are shown as a function of frequency. To use these MT data to investigate the Earth's structure, the MT data must be converted into a resistivity model as a function of depth and horizontal position. This is done using a mathematical process called inversion, which produces a model of subsurface resistivity that fits the measured MT data curves to a specified statistical misfit. To do this, the inversion program represents the resistivity structure of the Earth as a set of layers or cells that each have an associated electrical resistivity. The predicted MT response of this model is compared to the measured MT data curves. The resistivity model is refined in a series of iterations until the predicted MT response of the model matches the measured MT data to within a specified tolerance. The inversion of MT data can use 1D, 2D, and 3D approaches. The 1D approach is the simplest and assumes a resistivity model with a set of horizontal layers (Simpson and Bahr, 2005). The 2D approach uses a model where resistivity varies with depth and distance along a profile of MT stations (Simpson and Bahr, 2005). A limitation of the 2D approach is that it assumes that the resistivity structure is invariant in the direction perpendicular to the profile. This may be approximately true in some cases, but in general the resistivity structure of the crust and upper mantle varies in three directions. The 3D inversion approach makes no assumptions about the subsurface structure but requires a much greater number of parameters than the 1D or 2D inversion approaches to define the subsurface structure. This means that the computational cost of a 3D inversion is far greater than for 1D or 2D inversions.

All inversions are subject to non-uniqueness, which means that many resistivity models can satisfy the measured MT data to the same statistical tolerance. Many inversion algorithms impose the requirement of spatial smoothness on the resistivity model. Thus, the inversion algorithm seeks the smoothest model that is consistent with the measured MT data. This reduces the number of artifacts introduced into the resulting model. Non-uniqueness can also be minimized by applying knowledge of regional geology and using other types of data as constraints during inversion or interpretation.

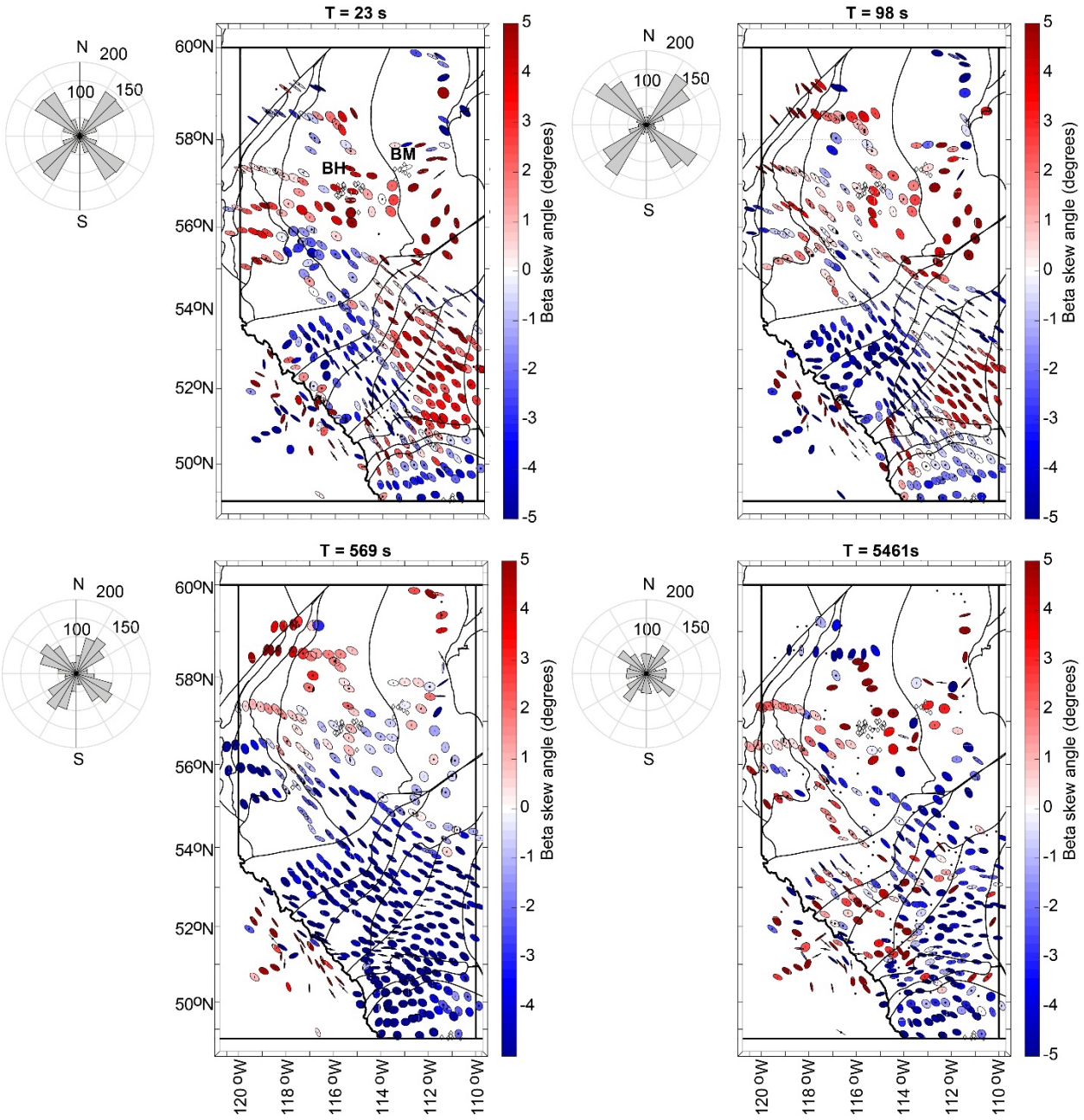

Figure 4. Phase tensors in Alberta at periods (T) of 23, 98, 569, and 5461 seconds (s). The rose diagrams show trends in the orientations of the major and minor axes of the phase tensors. Black dots indicate sites of magnetotelluric stations and white diamonds indicate individual kimberlite and similar intrusions. Thin black lines represent tectonic terrane boundaries (see Figure 1). Thick black lines represent the provincial borders. Abbreviations: BH, Buffalo Head Hills kimberlite field; BM, Birch Mountains kimberlite field.

The 3D inversion approach was used because the survey collected data from a grid of stations (Figure 1) and the phase tensors in Figure 4 showed that the resistivity structure of the subsurface is three dimensional. In this study, the 3D inversion approach was performed using the ModEM (Modular system for Electromagnetic inversion) code of Kelbert et al. (2014). This inversion process is computationally

demanding, requiring the use of high-performance computer clusters. Two resistivity models were obtained by the inversion of the MT data and are compared in this report.

The 2022 resistivity model, published by Wang and Unsworth (2022), includes all of the long-period MT data collected across Alberta prior to 2022 (Figure 1). The 2022 model was obtained by the following inversion procedure. The inversion began from a starting model that had a uniform resistivity of 100 Ω•m. The model was divided into cells that were 8 km wide in both the north-south and east-west directions. In the vertical direction, the first row of cells was assigned a thickness of 60 m and subsequent cell thicknesses increased geometrically by a factor of 1.2. This resulted in a total of 70 cells in the vertical direction. The starting model contained 198 by 136 by 70 cells. The inversion used data from 396 MT stations (in Alberta and southeastern British Columbia; Figure 1) and obtained a final root mean square (RMS) misfit value of 1.533 after 302 iterations (Figure 5). Topography was not included in this inversion. Error floors of 10% and 5% were applied to the diagonal and off-diagonal components of the impedance tensor, respectively, to handle noise in the data and avoid overfitting some data with small errors. Wang (2019) and Wang and Unsworth (2022) performed robust analyses of the sensitivity of the MT data to the various anomalies. The results of those studies showed the major conductors, including the BMC, were required to fit the measured MT data.

The 2023 resistivity model was obtained by an inversion of the original MT data and the additional MT data collected in 2022, from a total of 411 stations (in Alberta and southeastern British Columbia; Figure 1). The 2023 inversion used the same starting model and parameters as the 2022 model. The 2023 inversion obtained a final RMS misfit value of 1.4746 after 315 iterations (Figure 5). Again, topography was not included in this inversion.

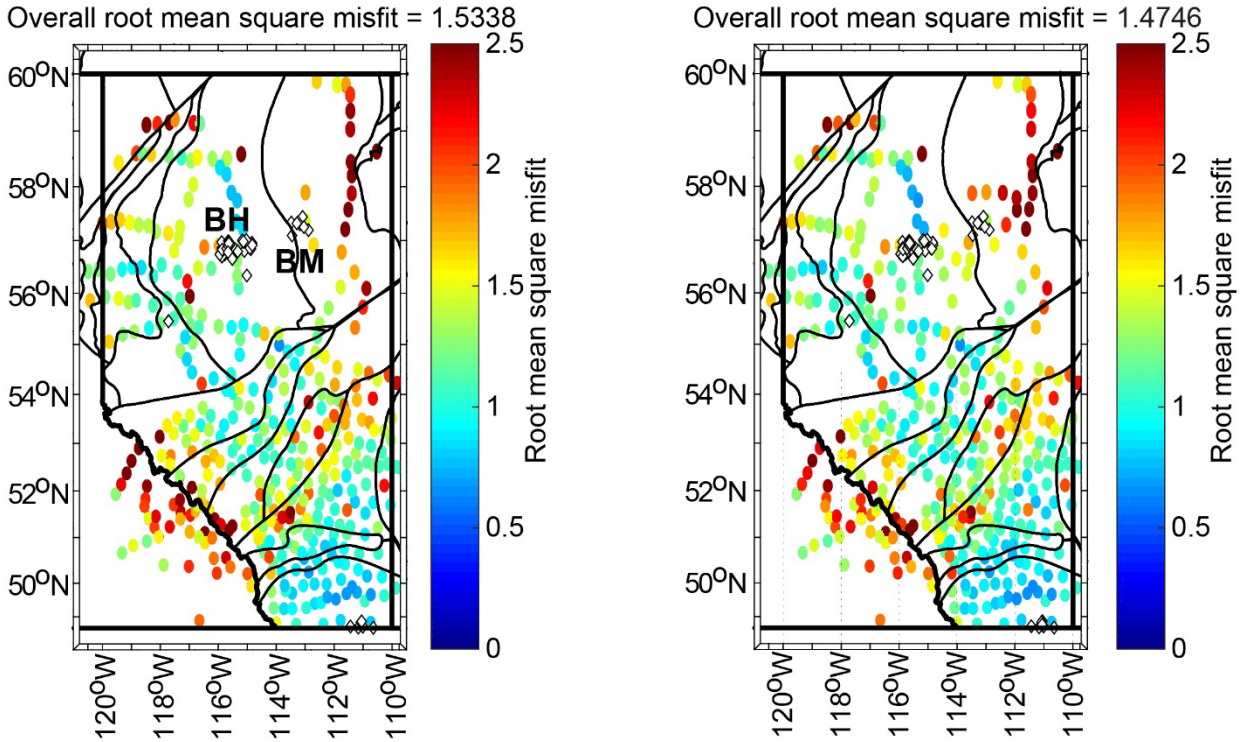

Figure 5. Root mean square misfit maps for the 2022 model (left) and 2023 model (right). The value for each station is represented by a coloured ellipse. White diamonds indicate individual kimberlite and similar intrusions. Thin black lines represent tectonic terrane boundaries (see Figure 1). Thick black lines represent the provincial borders. Abbreviations: BH, Buffalo Head Hills kimberlite field; BM, Birch Mountains kimberlite field.

A comparison of both resistivity models across all of Alberta is described below. However, given that the recently collected MT data focused on the Birch Mountains and Buffalo Head Hills kimberlite fields, this will remain the focus of the discussion in this report. Readers interested in the analysis and interpretation of the additional features and anomalies outside of this region are directed to Nieuwenhuis et al. (2014), Liddell et al. (2016), Wang et al. (2018), and Wang and Unsworth (2022).

6.1 Observations on the 2022 Model of Wang and Unsworth (2022)

Slices from the 2022 model are shown in Figures 6 (with comparable 2023 slices shown in Figure 7), 8 (with comparable 2023 slices shown in Figure 9), 10, and 11 and show the following:

- In the depth range 0–1 km bsl, a series of shallow conductors are located around both kimberlite fields (Figure 6). The features have resistivity values in the range of 1–30 Ω•m and can be identified as the sedimentary rocks of the WCSB. These WCSB conductors are more obvious farther south where the MT station coverage is denser. The WCSB is spatially continuous in both the north-south and east-west directions. However, it is not imaged as a horizontally continuous layer because of the relatively large distance between the MT stations. This phenomenon has been observed in the inversion models obtained in other MT studies, including the EarthScope project in the United States (Bedrosian, 2016).
- In the depth range 2–20 km bsl, the region around the Buffalo Head Hills kimberlite field is resistive with resistivity values in the range of 100–10 000 Ω•m (Figure 6). This can be interpreted as representing the crystalline rocks that underlie the WCSB. In contrast, around the Birch Mountains kimberlite field, a series of discrete 1–10 Ω•m conductors are present in the crystalline basement (Figure 6).
- In the depth range 20–70 km bsl, the same resistivity pattern as the 2–20 km bsl depth is observed. Beneath the Buffalo Head Hills kimberlite field, the crustal and upper mantle resistivity remains high. Beneath the Birch Mountains kimberlite field, the resistivity increases with depth but remains lower than beneath the Buffalo Head Hills region (Figure 6).
- Between 100 and 200 km bsl, a major north-south trending region of low resistivity (1–50 Ω•m), termed the BMC, is observed east and northeast of the Birch Mountains kimberlite field (Figure 8). North-south cross-sections of the model are displayed in Figure 10 and show that the BMC first appears at a depth of 100 km bsl. The southern edge dips steeply to the south of the Birch Mountains kimberlites (Figure 10). The northern edge dips northwards at a gentler angle until the boundary of the model (Figure 10). Slightly east of the Birch Mountains kimberlite field, the BMC appears to connect upwards with the shallow conductors located in the crust near the Birch Mountains kimberlite field and farther north near Fort Chipewyan (Figures 1, 10, and 11). Where MT station coverage is the densest, east of the Birch Mountains kimberlite field, a resistive block appears to interrupt these low resistivity structures. East-west cross-sections in Figure 11 show that the BMC appears as a conductive impingement on another otherwise resistive lithosphere. North of the Birch Mountains kimberlite field, this impingement rises to a depth of 100 km bsl; farther south it only rises to a depth of 180 km bsl.
- Starting at a depth of 150 km bsl, the BMC bends westwards until it underlies the Birch Mountains kimberlite field at a depth of 200 km bsl (Figures 8 and 11). The resistivity increases with depth until 250 km bsl where it merges with a regional scale 20–30 Ω•m conductor underlying most of northern Alberta, which can be identified as the asthenosphere (Figure 8). The lithospheric resistivity beneath the Buffalo Head Hills kimberlite field is the exact opposite of what is observed beneath the Birch Mountains kimberlite field. In fact, it distinctly remains the most resistive lithosphere in northern Alberta until the regional conductor at 250 km bsl is encountered (Figure 8).

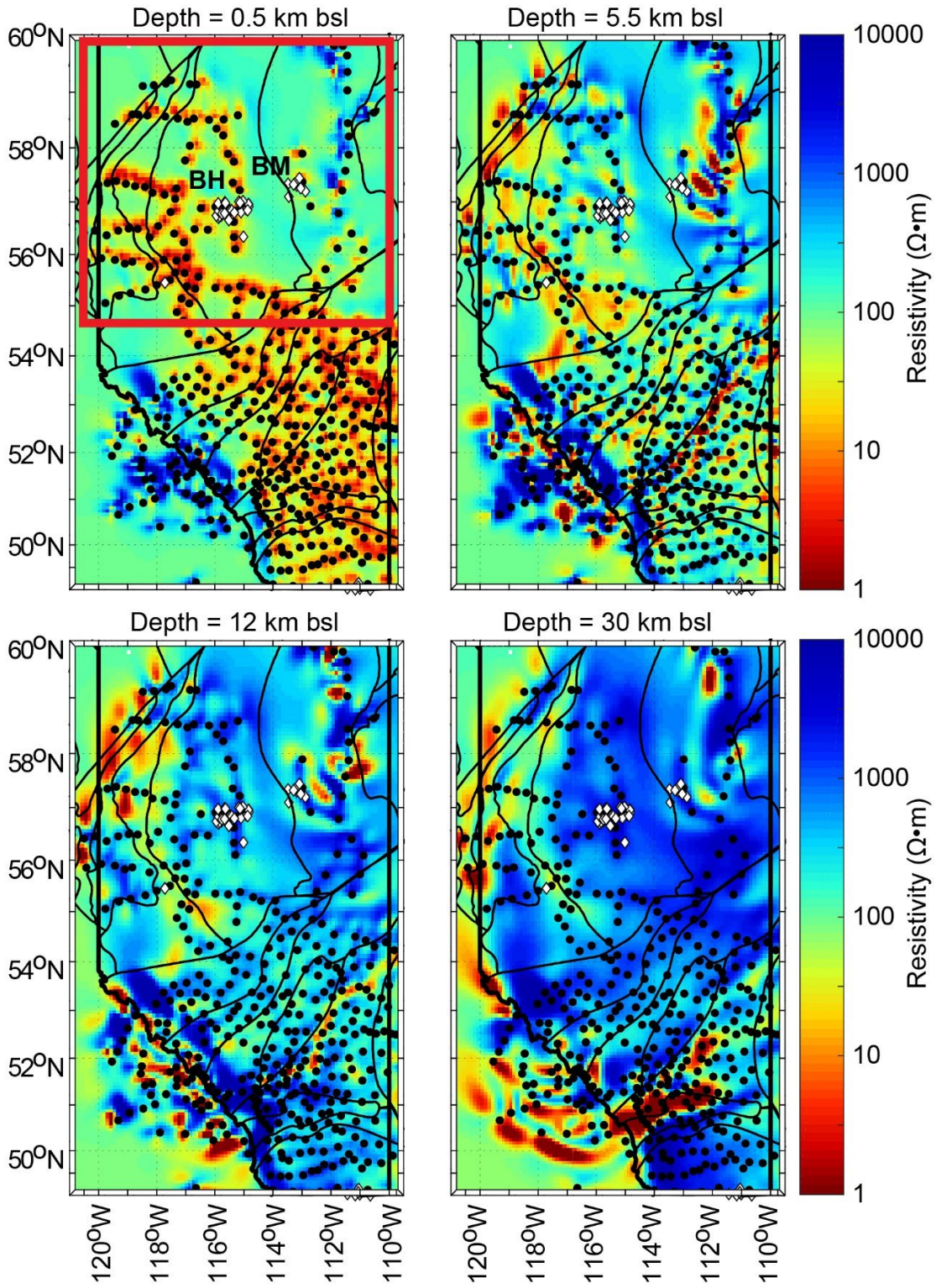

Figure 6. Horizontal model slices from the 2022 resistivity model at depths of 0.5, 5.5, 12, and 30 km below sea level. The red box in the upper left panel is the area shown in Figures 10, 11, and 13. Black dots indicate sites of magnetotelluric stations and white diamonds indicate individual kimberlite and similar intrusions. Thin black lines represent tectonic terrane boundaries (see Figure 1). Thick black lines represent the provincial borders. Abbreviations: Ω, ohm; BH, Buffalo Head Hills kimberlite field; BM, Birch Mountains kimberlite field.

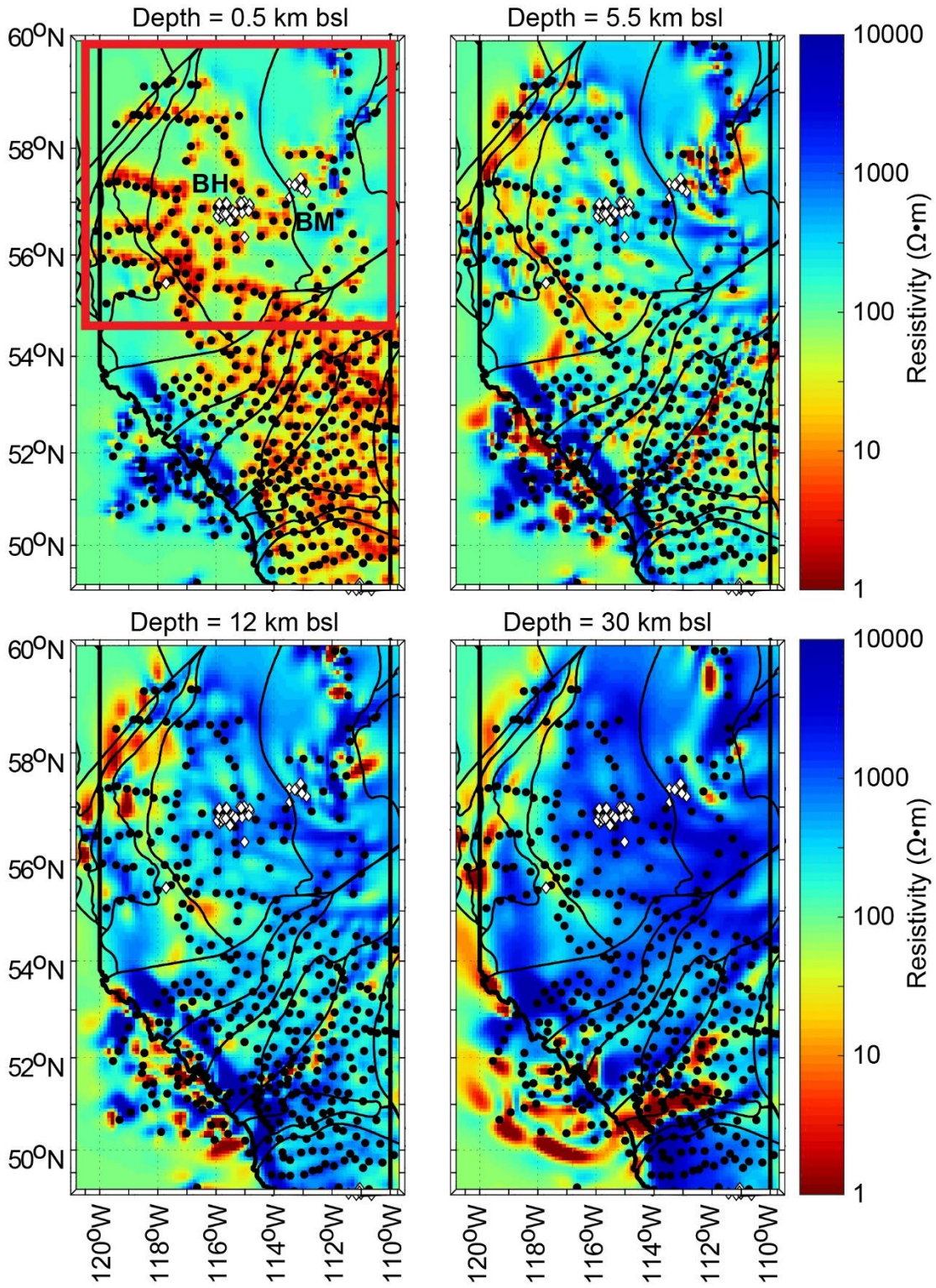

Figure 7. Horizontal model slices from the 2023 resistivity model at depths of 0.5, 5.5, 12, and 30 km below sea level. The red box in the upper left panel is the area shown in Figures 10 and 11. Black dots indicate sites of magnetotelluric stations and white diamonds indicate individual kimberlite and similar intrusions. Thin black lines represent tectonic terrane boundaries (see Figure 1). Thick black lines represent the provincial borders. Abbreviations: Ω, ohm; BH, Buffalo Head Hills kimberlite field; BM, Birch Mountains kimberlite field.

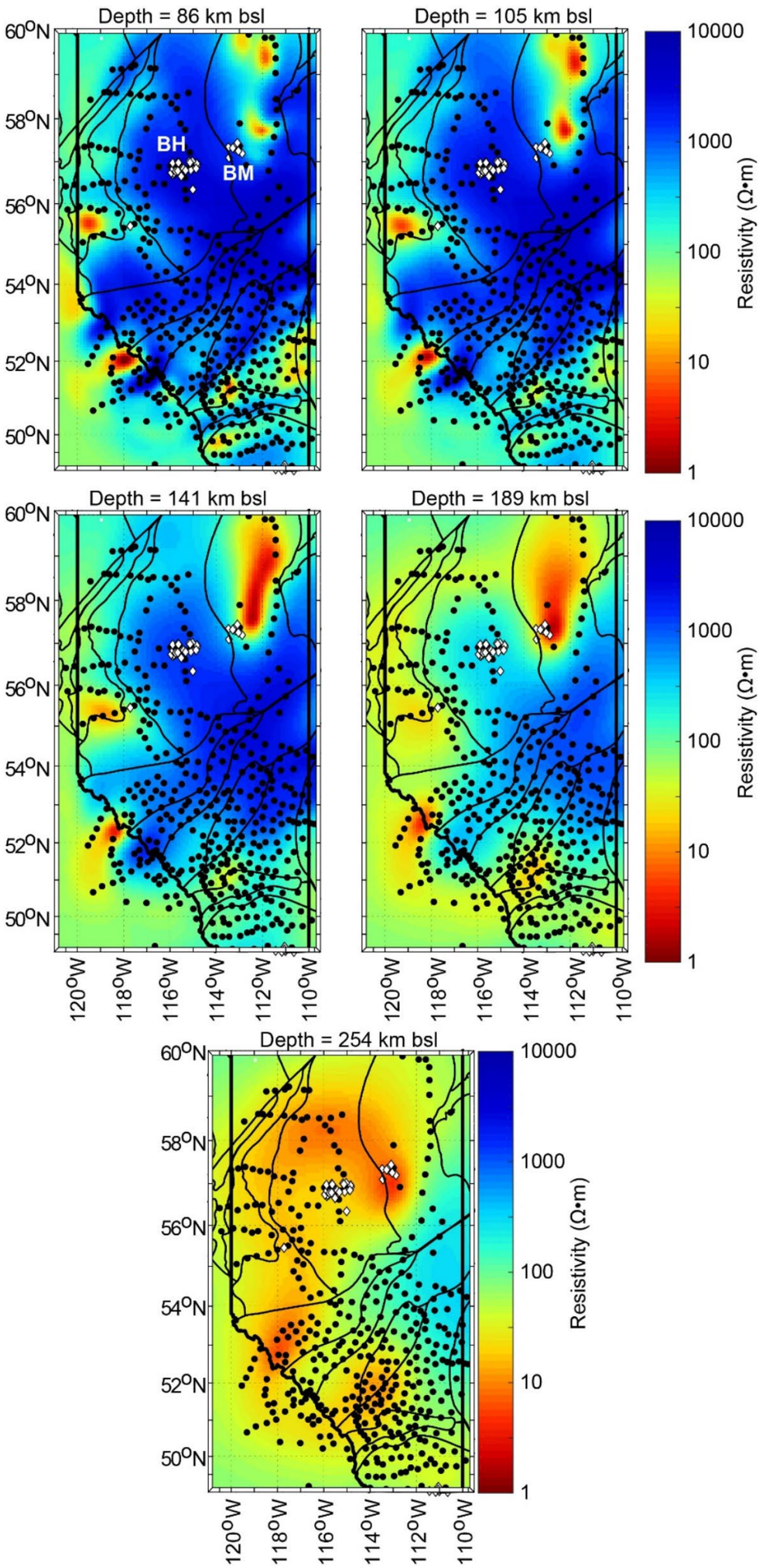

Figure 8. Horizontal model slices from the 2022 resistivity model at depths of 86, 105, 141, 189, and 254 km below sea level. Black dots indicate sites of magnetotelluric stations and white diamonds indicate individual kimberlite and similar intrusions. Thin black lines represent tectonic terrane boundaries (see Figure 1). Thick black lines represent the provincial borders. Abbreviations: Ω, ohm; BH, Buffalo Head Hills kimberlite field; BM, Birch Mountains kimberlite field.

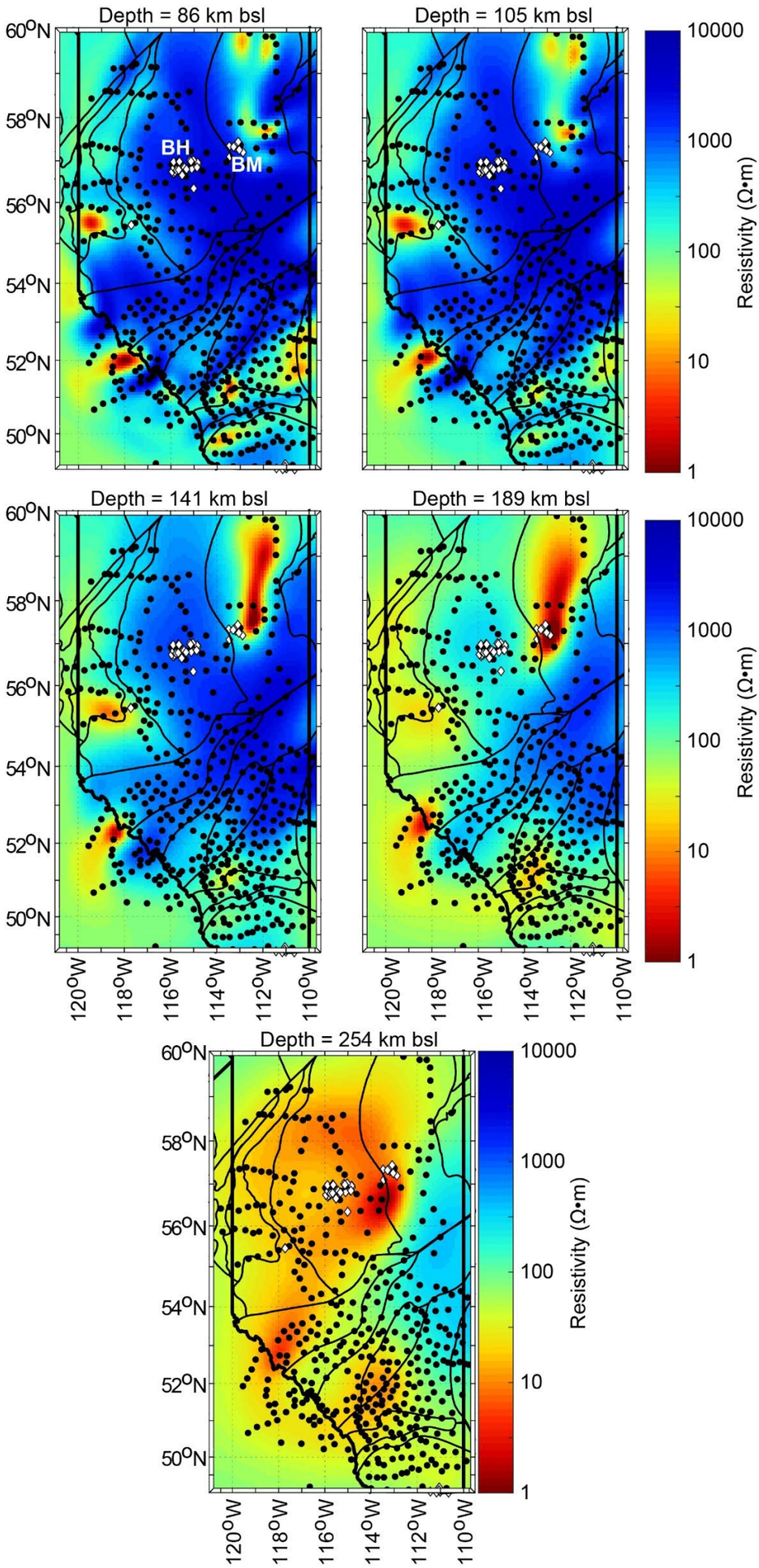

Figure 9. Horizontal model slices from the 2023 resistivity model at depths of 86, 105, 141, 189, and 254 km below sea level. Black dots indicate sites of magnetotelluric stations and white diamonds indicate individual kimberlite and similar intrusions. Thin black lines represent tectonic terrane boundaries (see Figure 1). Thick black lines represent the provincial borders. Abbreviations: Ω, ohm; BH, Buffalo Head Hills kimberlite field; BM, Birch Mountains kimberlite field.

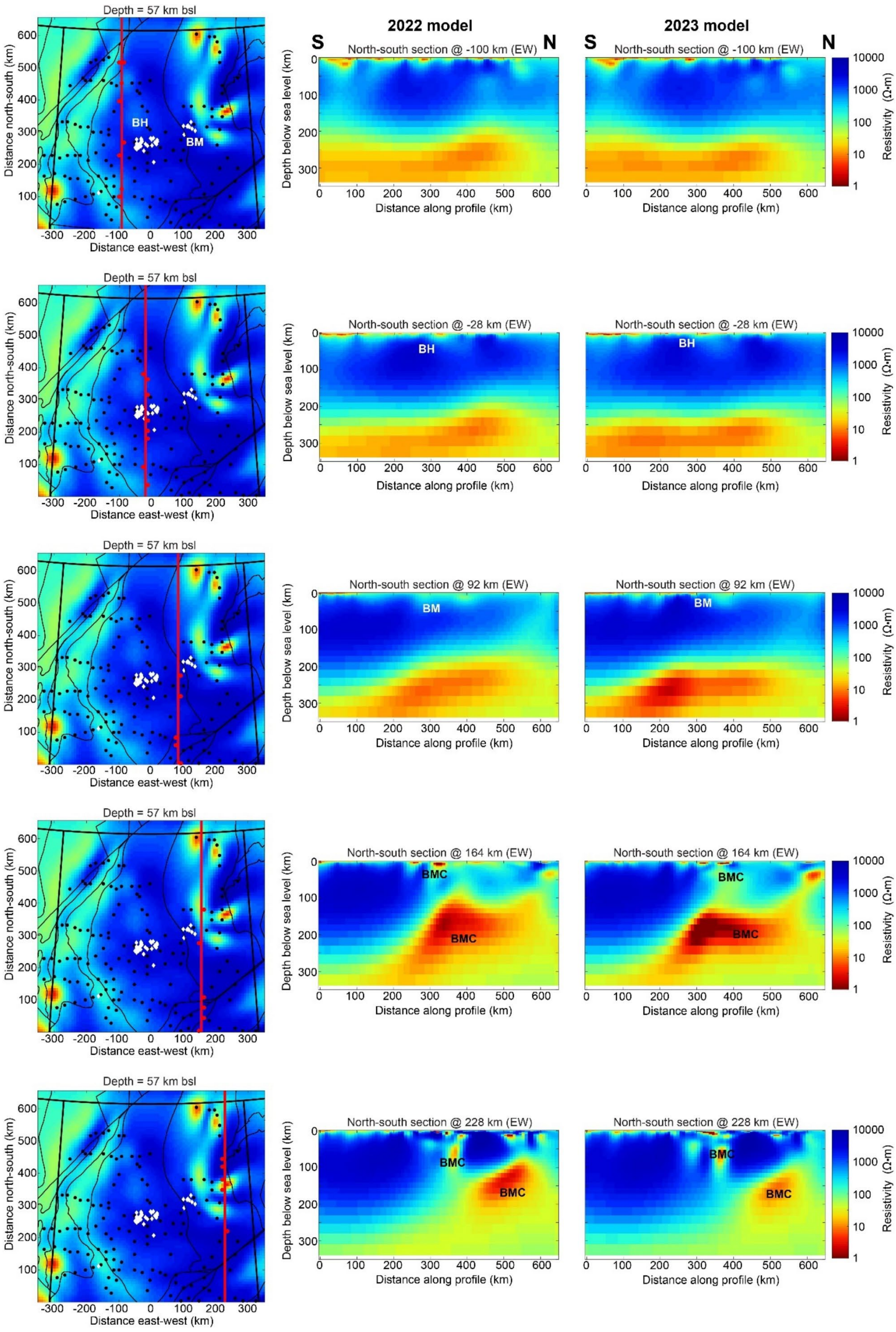

Figure 10. North-south vertical depth slices of the northern portion of the model region (outlined in Figure 6). The left column shows the model region, with the purple line showing the path of the slice. (black dots indicate sites of magnetotelluric stations and white diamonds indicate individual kimberlite and similar intrusions; thin black lines represent tectonic terrane boundaries [see Figure 1]; thick black lines represent the provincial borders). The centre column shows the slice from the 2022 resistivity model, the right column shows the slice from the 2023 resistivity model. Abbreviations: Ω, ohm; BH, Buffalo Head Hills kimberlite field; BM, Birch Mountains kimberlite field; BMC, Birch Mountains conductor; EW, east-west.

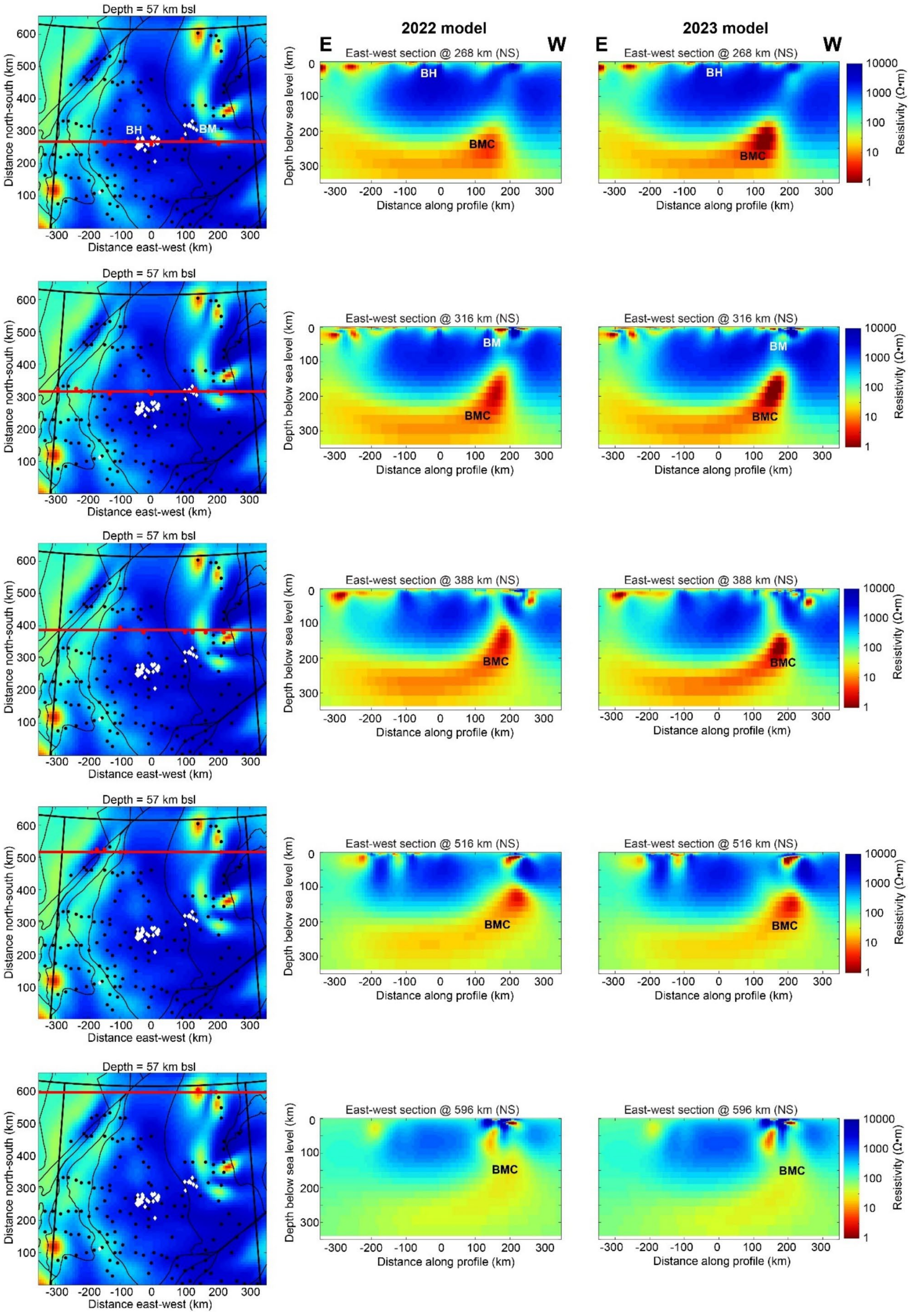

Figure 11. East-west vertical depth slices of the northern portion of the model region (outlined in Figure 6). The left column shows the model region, with the purple line showing the path of the slice (black dots indicate sites of magnetotelluric stations and white diamonds indicate individual kimberlite and similar intrusions; thin black lines represent tectonic terrane boundaries [see Figure 1; thick black lines represent the provincial borders). The centre column shows the slice from the 2022 resistivity model, the right column shows the slice from the 2023 resistivity model. Abbreviations: Ω, ohm; BH, Buffalo Head Hills kimberlite field; BM, Birch Mountains kimberlite field; BMC, Birch Mountains conductor; NS, north-south.

6.2 Observations on the New 2023 3D Resistivity Model

The new 3D resistivity model of Alberta generally shows the same features as those described in Section 6.1. This section will only discuss the differences observed between the two resistivity models.

At depths less than 6 km bsl, the new resistivity model shows that the shallow conductors east and northeast of the Birch Mountains kimberlite field are more numerous and smaller than in the 2022 model (Figure 7). At depths down to 12 km bsl, the conductor just east of the Birch Mountains kimberlite field evident in Figure 6 is not longer evident (Figure 7). Below a depth of 12 km bsl, the resistivity structure is very similar to the 2022 model, and the BMC is still present in the depth range 80–200 km bsl (Figures 8 and 9). However, the spatial extent of the low resistivity anomaly has decreased, and the anomaly is narrower than in the 2022 model (compare Figures 8 and 9). In the east-west and north-south cross-sections, there are limited differences between the two models (Figures 10 and 11).

7 Interpretation

Summary Figure 12a–d displays the results of both models and a comparison of them to seismic anomalies in the region. The new 2023 3D resistivity model is generally similar to the model previously published by Wang and Unsworth (2022). The major change in the 2023 model is that the BMC is imaged as a sharper, narrower feature than in the 2022 model. Additionally, in the new model the BMC does not extend as far west towards the Buffalo Head Hills kimberlite field as in the 2022 model. The presence of the BMC beneath the Birch Mountains kimberlite field and the absence of a conductor beneath the Buffalo Head Hills kimberlite field is significant. Seismic data also show a similar difference in lithospheric structure, with a low velocity anomaly beneath the Birch Mountains kimberlite field and no anomaly beneath the Buffalo Head Hills kimberlite field (Figure 12b; Chen et al., 2020). An isosurface plot of the BMC and asthenosphere conductors shows a remarkable correspondence between the low velocity anomaly of Chen et al. (2020) and the resistivity model (Figure 13). Wang and Unsworth (2022) noted that the kimberlites of the Birch Mountains kimberlite field either sampled warmer temperature zones or originated at shallower depths than kimberlites found in the Buffalo Head Hills kimberlite field (Eccles, 2011). Wang and Unsworth (2022) integrated their results with constraints from (1) the seismic study of Chen et al. (2020; Figure 12c); (2) xenolith studies of Burwash et al. (2000); and (3) a petrological study of Eccles et al. (2004). Wang and Unsworth (2022) suggested that both the low resistivity and low velocity seismic anomalies associated with the BMC may reflect either (1) intense metasomatic modification that introduced hydrous minerals such as phlogopite or amphibole or (2) extensive enrichment of the lithosphere beneath the Birch Mountains kimberlite field. They also suggest that the resistive lithosphere beneath the Buffalo Head Hills kimberlite field reflects an absence of this modification or enrichment, and instead represents dry and depleted lithosphere.

Recent laboratory experiments allow a quantitative analysis of the lithospheric resistivity values determined from the MT data. The presence of hydrous minerals can produce both low resistivity and low velocity seismic anomalies (Selway, 2014, 2018; Rader et al., 2015). The seismic anomalies associated with the BMC correspond to an ~2% velocity reduction in shear wave velocity (Chen et al., 2018, 2020), which requires the presence of 5–7% phlogopite or 10% amphibole (Rader et al., 2015). Modelling of these hydrous phases in a mantle of a similar age and thermal structure, located farther east in Saskatchewan, showed that phlogopite can explain the resistivity values of the BMC in the upper mantle (Chase and Unsworth, 2022). Amphibole is not a viable explanation for the low resistivity anomaly because this mineral phase is not stable at pressures greater than 3 GPa, which occur at a depth of around 100 km and the BMC is deeper than this. At shallower depths, the modelling of Chase and Unsworth (2022) suggest phlogopite becomes less viable as an explanation for the low resistivity anomaly because 10–25% phlogopite by volume would be required to produce the resistivity of 1–10 Ω•m observed in the BMC. This amount of phlogopite would produce seismic anomalies greater than those observed in the region (Rader et al., 2015; Chen et al., 2018, 2020).

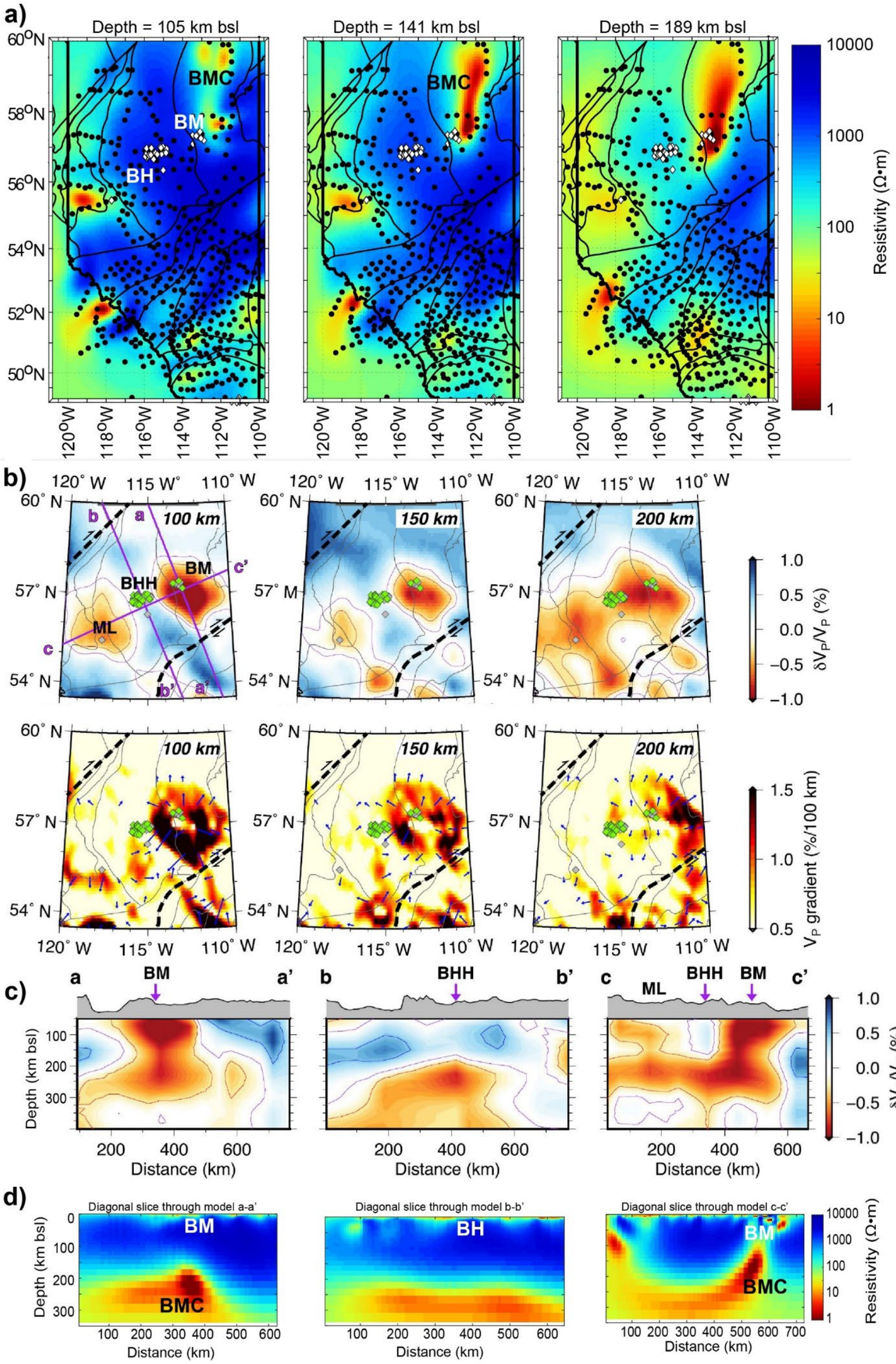

Figure 12. (a) Horizontal model slices from the 2022 resistivity model showing the Birch Mountains conductor (BMC) at depths of 105, 141, and 189 km below sea level (bsl). Black dots indicate sites of magnetotelluric stations and white diamonds indicate individual kimberlite and similar intrusions. Thin black lines represent terrane boundaries (see Figure 1). Thick black lines represent the provincial borders. (b) Horizontal model slices from the seismic model of Chen et al. (2020) at depths of 100, 150, and 200 km bsl, similar depths to those shown in (a). The slices show a low velocity anomaly beneath the Birch Mountains kimberlite field (BM) and no anomaly beneath Buffalo Head Hills kimberlite field (BH/BHH). Green and grey diamonds indicate diamondiferous and nondiamondiferous kimberlite fields, respectively; black dashed lines indicate the Great Slave Lake shear zone and Snowbird tectonic zone; blue arrows indicate the directions of the largest velocity gradients; grey lines represent terrane boundaries; and purple lines indicate the locations of profiles shown in (c). (c) Vertical model slices from the seismic model of Chen et al. (2020) showing the low velocity anomaly with depth. The locations of the profiles are shown in the upper left-hand model slice in (b). (d) Vertical model slices from the 2023 resistivity model taken over the same profile locations as (c). Note that the vertical scale of (c) is different from (d). Abbreviations: Ω, ohm; ML, Mountain Lake kimberlite field; Vp, seismic p-wave velocity.

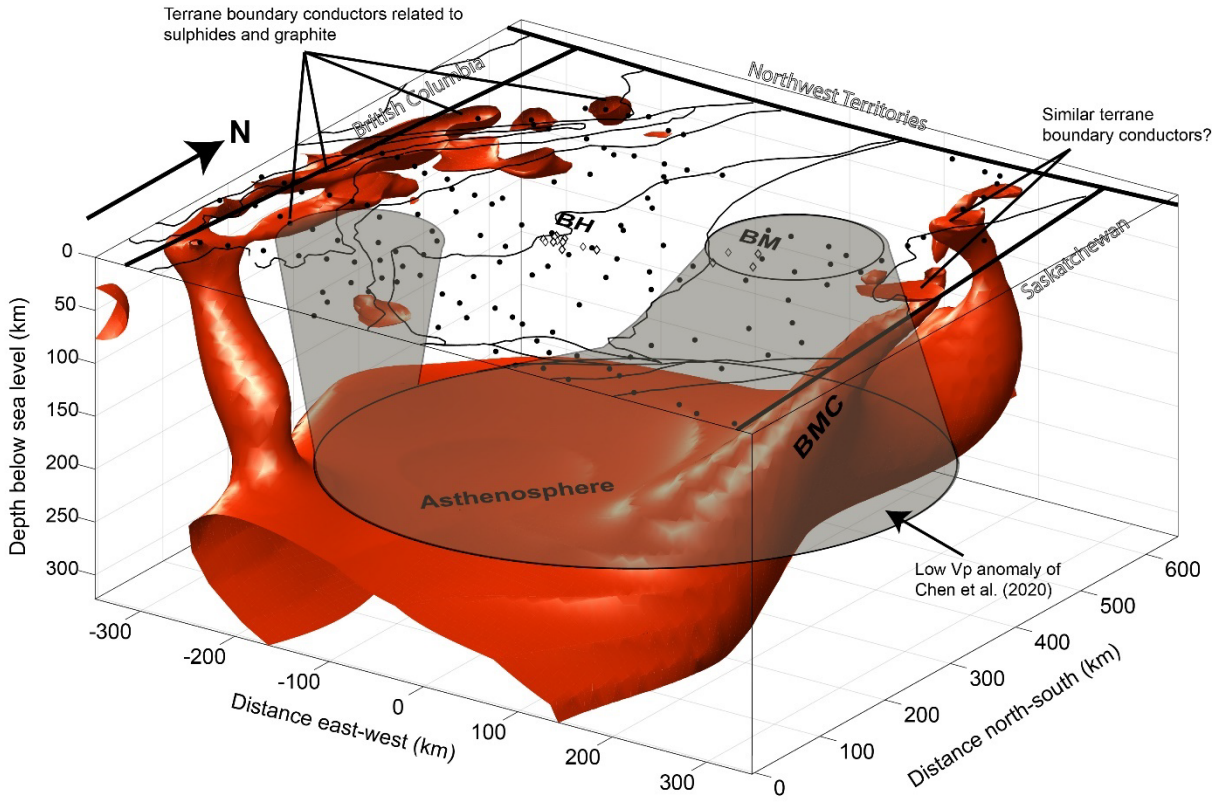

Figure 13. Isosurface plot from the 2023 resistivity model at 30 ohm•metres (Ω•m) showing the geometry of the low resistivity anomalies in the study area (see Figure 6 for location). The shallow conductors in the west were interpreted by Türkoğlu et al. (2009) and Wang et al. (2018). Black dots indicate sites of magnetotelluric stations and white diamonds indicate individual kimberlite and similar intrusions. Abbreviations: BH, Buffalo Head Hills kimberlite field; BM, Birch Mountains kimberlite field; BMC, Birch Mountains conductor; Vp, seismic p-wave velocity.

The alternative hypothesis suggested by Wang and Unsworth (2022) to explain the low resistivity of the BMC was lithospheric enrichment. This would reduce seismic velocities (Deen et al., 2006) and is consistent with the model of Chen et al. (2018, 2020). However, enrichment is unlikely to produce low resistivity anomalies unless the mantle minerals are also enriched in water in the form of H^+ (Selway, 2018). Wang and Unsworth (2022) modelled the resistivity effects produced by enrichment of olivine in water and concluded that the observed BMC resistivity values could not be explained with this conduction mechanism. Chase and Unsworth (2022), again farther east in Saskatchewan, showed that the resistivity values observed in the BMC could be reproduced in the lowermost lithospheric mantle via water enrichment if the lithosphere is modelled with a more complex multiphase mineralogy. However, similar to phlogopite, water enrichment becomes a less viable mechanism at depths shallower than 100–150 km because the water concentrations required would exceed the solubility limits of mantle minerals (Padrón-Navarta and Hermann, 2017; Chase and Unsworth, 2022). A direct assessment of the resistivity of the BMC using the updated techniques of Chase and Unsworth (2022) will be performed for the lithosphere beneath northern Alberta in the near future.

In the isosurface plot shown in Figure 13, the BMC and asthenosphere conductors connect to shallower upper crustal conductors located to both the east and west of the two kimberlite fields. The western series of shallow conductors has been previously interpreted as reflecting sulphides or graphite deposited during terrane assembly and associated metamorphism (Türkoğlu et al., 2009; Wang and Unsworth, 2022). The eastern conductors are offset from the Birch Mountains kimberlite field by 50–100 km (Figure 13), and

their exact nature is unknown. However, many of the conductivity mechanisms that can help to explain low resistivity anomalies in the mantle have minimal effect on resistivity values in the crust (Chase and Unsworth, 2022). The notable exceptions to this are sulphides and graphite. As a result, it remains plausible that the genetic origin of the eastern conductors is similar to those found to the west (Figure 13). A direct assessment of these shallow conductors will also be performed in the near future.

In summary, the mechanisms suggested by Wang and Unsworth (2022) to explain BMC resistivity values in the lower lithospheric mantle remain plausible based on mantle resistivity modelling and constraints from seismic and xenolith data. However, rigorous mantle resistivity modelling has not been performed and will benefit from the additional data collected at MT stations in 2022 and discussed in this report. Further, as noted by Wang and Unsworth (2022), the connection of the BMC to the asthenosphere, the northward extension of the BMC, and the vertical geometry of the BMC remains unexplained. The genetic relationship of the BMC and other regional conductors to the diamond potential of both the Buffalo Head Hills and Birch Mountains kimberlite fields has also not been investigated. Finally, the connection between the BMC, the asthenosphere conductor, and the shallow conductors east and west of the kimberlite fields remains unclear. In future research, analysis of these new MT data will be used to examine these unanswered questions.

8 Conclusions

In this study, a preliminary three-dimensional resistivity model has been developed for the Buffalo Head Hills and Birch Mountains kimberlite fields using long-period magnetotelluric (MT) data. The main objective of the study was to evaluate how the recently collected MT data have improved imaging of a large lithospheric mantle conductor beneath the Birch Mountains kimberlite field and the lack of a conductor beneath the Buffalo Head Hills kimberlite field. The existence, or lack of, an anomaly near or underneath a kimberlite field has previously been inferred to be related to the diamond potential of the kimberlites. This study shows the conductor beneath the Birch Mountains kimberlite field is narrower than previously imaged and does not extend significantly westward towards the Buffalo Head Hills kimberlite field. Further, the lithosphere beneath the Buffalo Head Hills kimberlite field is among the most resistive lithosphere in northern Alberta. Tentative modelling results suggest that interpretations by other authors that the Birch Mountains conductor (BMC) could represent a region of lithosphere enrichment or hydrous minerals remain valid. A more extensive investigation of the causes of the low mantle resistivity will be undertaken in order to fully evaluate which conductivity enhancing mechanisms could explain the low resistivity of the BMC. These results will be compared with regional xenolith analytical and mantle petrological data to determine if there is a genetic relationship between the anomalies and kimberlite diamond potential.

9 References

Banas, A., Stachel, T., Muehlenbachs, K. and McCandless, T.E. (2007): Diamonds from the Buffalo Head Hills, Alberta: formation in a non-conventional setting; Lithos, v. 93, no. 1–2, p. 199–213, doi:10.1016/j.lithos.2006.07.001.

Bedrosian, P.A. (2016): Making it and breaking it in the Midwest: continental assembly and rifting from modeling of EarthScope magnetotelluric data; Precambrian Research, v. 278, p. 337–361, doi:10.1016/j.precamres.2016.03.009.

Bettac, S.P., Unsworth, M.J., Pearson, D.G. and Craven, J. (2023): New constraints on the structure and composition of the lithospheric mantle beneath the Slave craton, NW Canada from 3-D magnetotelluric data–origin of the Central Slave Mantle Conductor and possible evidence for lithospheric scale fluid flow; Tectonophysics, v. 851, art. 229760, doi:10.1016/j.tecto.2023.229760.

Boerner, D.E., Kurtz, R.D., Craven, J.A., Ross, G.M. and Jones, F.W. (2000): A synthesis of electromagnetic studies in the Lithoprobe Alberta Basement Transect: constraints on Paleoproterozoic indentation tectonics; Canadian Journal of Earth Sciences, v. 37, no. 11, p. 1509–1534, doi:10.1139/e00-063.

Booker, J.R. (2014): The magnetotelluric phase tensor: a critical review; Surveys in Geophysics, v. 35, p. 7–40.

Burwash, R.A., Krupička, J. and Wijbrans, J.R. (2000): Metamorphic evolution of the Precambrian basement of Alberta; The Canadian Mineralogist, v. 38, no. 2, p. 423–434, doi:10.2113/gscanmin.38.2.423.

Caldwell, T.G., Bibby, H.M. and Brown, C. (2004): The magnetotelluric phase tensor; Geophysical Journal International, v. 158, no. 2, p. 457–469, doi:10.1111/j.1365-246X.2004.02281.x.

Chacko, T., De, S.K., Creaser, R.A. and Muehlenbachs, K. (2000): Tectonic setting of the Taltson magmatic zone at 1.9–2.0 Ga: a granitoid-based perspective; Canadian Journal of Earth Sciences, v. 37, no. 11, p. 1597–1609, doi:10.1139/e00-029.

Chase, B. and Unsworth, M.J. (2022): Results from a long-period magnetotelluric (MT) study of the Fort à la Corne kimberlite field and surrounding Trans-Hudson Orogen, Saskatchewan; AGU Fall Meeting 2022, Chicago, Illinois, December 12–16, 2022, Abstracts, v. 2022, p. GP35B-0355.

Chen, Y., Gu, Y.J. and Hung, S.H. (2018): A new appraisal of lithospheric structures of the Cordillera-Craton Boundary Region in western Canada, Tectonics, v. 37, no. 9, p. 3207–3228, doi:10.1029/2018TC004956.

Chen, Y., Gu, Y.J., Heaman, L.M., Wu, L., Saygin, E. and Hung, S.H. (2020): Reconciling seismic structures and Late Cretaceous kimberlite magmatism in northern Alberta, Canada; Geology, v. 48, no. 9, p. 872–876, doi:10.1130/G47163.1.

Czas, J., Pearson, D.G., Stachel, T., Kjarsgaard, B.A. and Read, G.H. (2020): A Palaeoproterozoic diamond-bearing lithospheric mantle root beneath the Archean Sask Craton, Canada; Lithos, v. 356, 105301, doi:10.1016/j.lithos.2019.105301.

Deen, T.J., Griffin, W.L., Begg, G., O'Reilly, S.Y., Natapov, L.M. and Hronsky, J. (2006): Thermal and compositional structure of the subcontinental lithospheric mantle: derivation from shear wave seismic tomography; Geochemistry, Geophysics, Geosystems, v. 7, no. 7, art. Q07003, 20 p., doi:10.1029/2005GC001120.

Eaton, D.W., Darbyshire, F., Evans, R.L., Grütter, H., Jones, A.G. and Yuan, X. (2009): The elusive lithosphere–asthenosphere boundary (LAB) beneath cratons; Lithos, v. 109, no. 1–2, p. 1–22, doi:10.1016/j.lithos.2008.05.009.

Eccles, D.R. (2011): Northern Alberta kimberlite province: the first 20 years; Energy Resources Conservation Board, ERCB/AGS Bulletin 65, 116 p., URL <https://ags.aer.ca/publication/bul-065> [July 2023].

Eccles, D.R. and Simonetti, A. (2008): A study of peridotitic garnet xenocryst compositions from selected ultramafic bodies in the northern Alberta kimberlite province: implications for mantle stratigraphy and garnet classification; Energy Resources Conservation Board, ERCB/AGS Earth Sciences Report 2008-01, 40 p., URL <https://ags.aer.ca/publication/esr-2008-01> [July 2023].

Eccles, D.R., Heaman, L.M., Luth, R.W. and Creaser, R.A. (2004): Petrogenesis of the Late Cretaceous northern Alberta kimberlite province; Lithos, v. 76, no. 1–4, p. 435–459, doi:10.1016/j.lithos.2004.03.046.

Frost, D.J. and McCammon, C.A. (2008): The redox state of Earth's mantle; Annual Review of Earth and Planetary Sciences, v. 36, p. 389–420, doi:10.1146/annurev.earth.36.031207.124322.

Hanneson, C. and Unsworth, M.J. (2023): Regional-scale resistivity structure of the middle and lower crust and uppermost mantle beneath the southeastern Canadian Cordillera and insights into its causes; Geophysical Journal International, v. 234, no. 3, p. 2032–2052, doi:10.1093/gji/ggad183.

Hoffman, P.F. (1988): United plates of America, the birth of a craton: Early Proterozoic assembly and growth of Laurentia; Annual Review of Earth and Planetary Sciences, v. 16, no. 1, p. 543–603, doi:10.1146/annurev.ea.16.050188.002551.

Jones, A.G., Ledo, J. and Ferguson, I.J. (2005): Electromagnetic images of the Trans-Hudson orogen: the North American Central Plains anomaly revealed; Canadian Journal of Earth Sciences, v. 42, no. 4, p. 457–478, doi:10.1139/e05-018.

Kelbert, A., Meqbel, N., Egbert, G.D. and Tandon, K. (2014): ModEM: a modular system for inversion of electromagnetic geophysical data; Computers & Geosciences, v. 66, p. 40–53, doi:10.1016/j.cageo.2014.01.010.

Kravchinsky, V.A., Eccles, D.R., Zhang, R. and Cannon, M. (2009): Paleomagnetic dating of the northern Alberta kimberlites; Canadian Journal of Earth Sciences, v. 46, no. 4, p. 231–245, doi:10.1139/E09-016.

Liddell, M., Unsworth, M. and Pek, J. (2016): Magnetotelluric imaging of anisotropic crust near Fort McMurray, Alberta: implications for engineered geothermal system development; Geophysical Journal International, v. 205, no. 3, p. 1365–1381, doi:10.1093/gji/ggw089.

Liu, L., Morgan, J.P., Xu, Y. and Menzies, M. (2018): Craton destruction 1: cratonic keel delamination along a weak midlithospheric discontinuity layer; Journal of Geophysical Research: Solid Earth, v. 123, no. 11, p. 10 040–10 068, doi:10.1029/2017JB015372.

Nieuwenhuis, G., Unsworth, M.J., Pana, D., Craven, J. and Bertrand, E. (2014): Three-dimensional resistivity structure of southern Alberta, Canada: implications for Precambrian tectonics; Geophysical Journal International, v. 197, no. 2, p. 838–859, doi:10.1093/gji/ggu068.

Özaydın, S. and Selway, K. (2022): The relationship between kimberlitic magmatism and electrical conductivity anomalies in the mantle; Geophysical Research Letters, v. 49, no. 18, art. e2022GL099661, 11 p., doi:10.1029/2022GL099661.

Padrón-Navarta, J.A. and Hermann, J. (2017): A subsolidus olivine water solubility equation for the Earth's upper mantle; Journal of Geophysical Research: Solid Earth, v. 122, no. 12, p. 9862–9880, doi:10.1002/2017JB014510.

Pilkington, M., Miles, W.F., Ross, G.M. and Roest, W.R. (2000): Potential-field signatures of buried Precambrian basement in the Western Canada Sedimentary Basin; Canadian Journal of Earth Sciences, v. 37, no. 11, p. 1453–1471, doi:10.1139/e00-020.

Rader, E., Emry, E., Schmerr, N., Frost, D., Cheng, C., Menard, J., Yu, C. and Geist, D. (2015): Characterization and petrological constraints of the midlithospheric discontinuity; Geochemistry, Geophysics, Geosystems, v. 16, no. 10, p. 3484–3504, doi:10.1002/2015GC005943.

Ross, G.M. (2002): Evolution of Precambrian continental lithosphere in Western Canada: results from Lithoprobe studies in Alberta and beyond; Canadian Journal of Earth Sciences, v. 39, no. 3, p. 413–437, doi:10.1139/e02-012.

Ross, G.M. and Eaton, D.W. (2002): Proterozoic tectonic accretion and growth of western Laurentia: results from Lithoprobe studies in northern Alberta; Canadian Journal of Earth Sciences, v. 39, no. 3, p. 313–329, doi:10.1139/e01-081.

Ross, G.M., Mariano, J. and Dumont, R. (1994): Was Eocene magmatism widespread in the subsurface of southern Alberta? Evidence from new aeromagnetic anomaly data; *in* 1994 LITHOPROBE Alberta basement transects workshop, LITHOPROBE Secretariat, University of British Columbia, LITHOPROBE Report No. 37, p. 240–249.

Russell, J.K., Sparks, R.S.J. and Kavanagh, J.L. (2019): Kimberlite volcanology: transport, ascent, and eruption; Elements, v. 15, no. 6, p. 405–410, doi:10.2138/gselements.15.6.405.

Selway, K. (2014): On the causes of electrical conductivity anomalies in tectonically stable lithosphere; Surveys in Geophysics, v. 35, p. 219–257, doi:10.1007/s10712-013-9235-1.

Selway, K. (2018): Electrical discontinuities in the continental lithosphere imaged with magnetotellurics; Chapter 5 *in* Lithospheric Discontinuities, H. Yuan and B. Romanowicz (ed.), American Geophysical Union, p. 89–109, doi:10.1002/9781119249740.ch5.

Simpson, F. and Bahr, K. (2005): Practical magnetotellurics; Cambridge University Press, Cambridge, United Kingdom, 270 p.

Skelton, D., Clements, B., McCandless, T.E., Hood, C., Aulbach, S., Davies, R. and Boyer, L.P. (2003): The Buffalo Head Hills kimberlite province, Alberta; *in* Slave Province and Northern Alberta Field Trip Guidebook, B.A. Kjarsgaard (ed.), 8th International Kimberlite Conference, Victoria, Canada, June 22–27, 2003, p. 11–19.

Stachel, T. and Luth, R.W. (2015): Diamond formation—where, when and how?; Lithos, v. 220, p. 200–220, doi:10.1016/j.lithos.2015.01.028.

Türkoğlu, E., Unsworth, M. and Pană, D. (2009): Deep electrical structure of northern Alberta (Canada): implications for diamond exploration; Canadian Journal of Earth Sciences, v. 46, no. 2, p. 139–154, doi:10.1139/E09-009.

Wang, E. (2019): Multidimensional magnetotelluric studies of the Precambrian Alberta basement; Ph.D. thesis, University of Alberta, 397 p., doi:10.7939/r3-sctk-1z12.

Wang, E. and Unsworth, M. (2022): Three-dimensional crustal and upper-mantle resistivity structure of Alberta, Canada: implications for Precambrian tectonics; Geophysical Journal International, v. 230, no. 3, p. 1679–1698, doi:10.1093/gji/ggac128.

Wang, E., Unsworth, M. and Chacko, T. (2018): Geoelectric structure of the Great Slave Lake shear zone in northwest Alberta: implications for structure and tectonic history; Canadian Journal of Earth Sciences, v. 55, no. 3, p. 295–307, doi:10.1139/cjes-2017-0067.

Zhang, B. and Yoshino, T. (2017): Effect of graphite on the electrical conductivity of the lithospheric mantle; Geochemistry, Geophysics, Geosystems, v. 18, no. 1, p. 23–40, doi:10.1002/2016GC006530.

Appendix 1 – Raw Data from the 2022 Magnetotelluric Stations

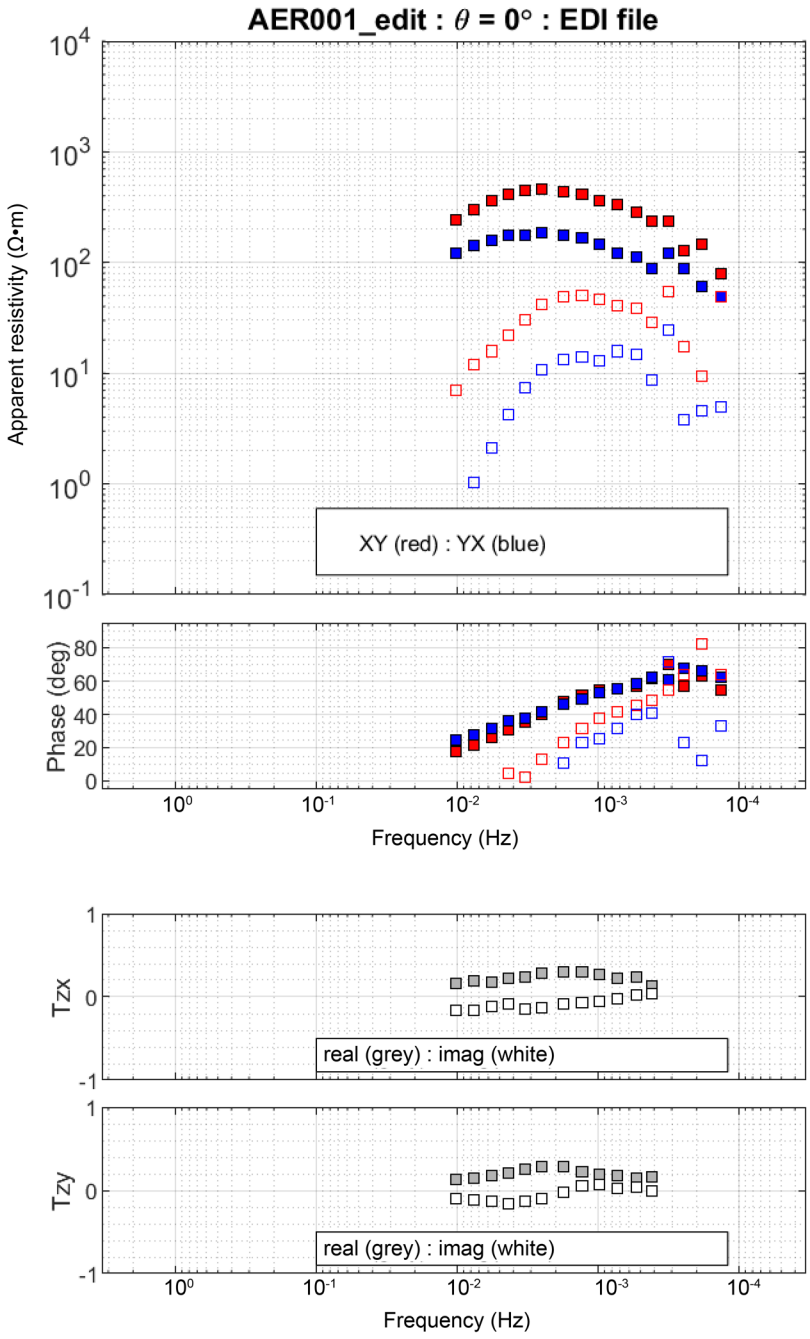

Figure 14. Data from station AER 001 (lat. 55.83°N, long. 114.16°W). In the top two panels, the solid red boxes are the XY component of the impedance tensor, solid blue boxes are the YX component, open red boxes are the XX component, and open blue boxes are the YY component. In the bottom two panels, the grey and white boxes are the real (in-phase) and the imaginary (imag; out-of-phase) components of the tipper (T), respectively. Abbreviations: Ω, ohms; deg, degrees.

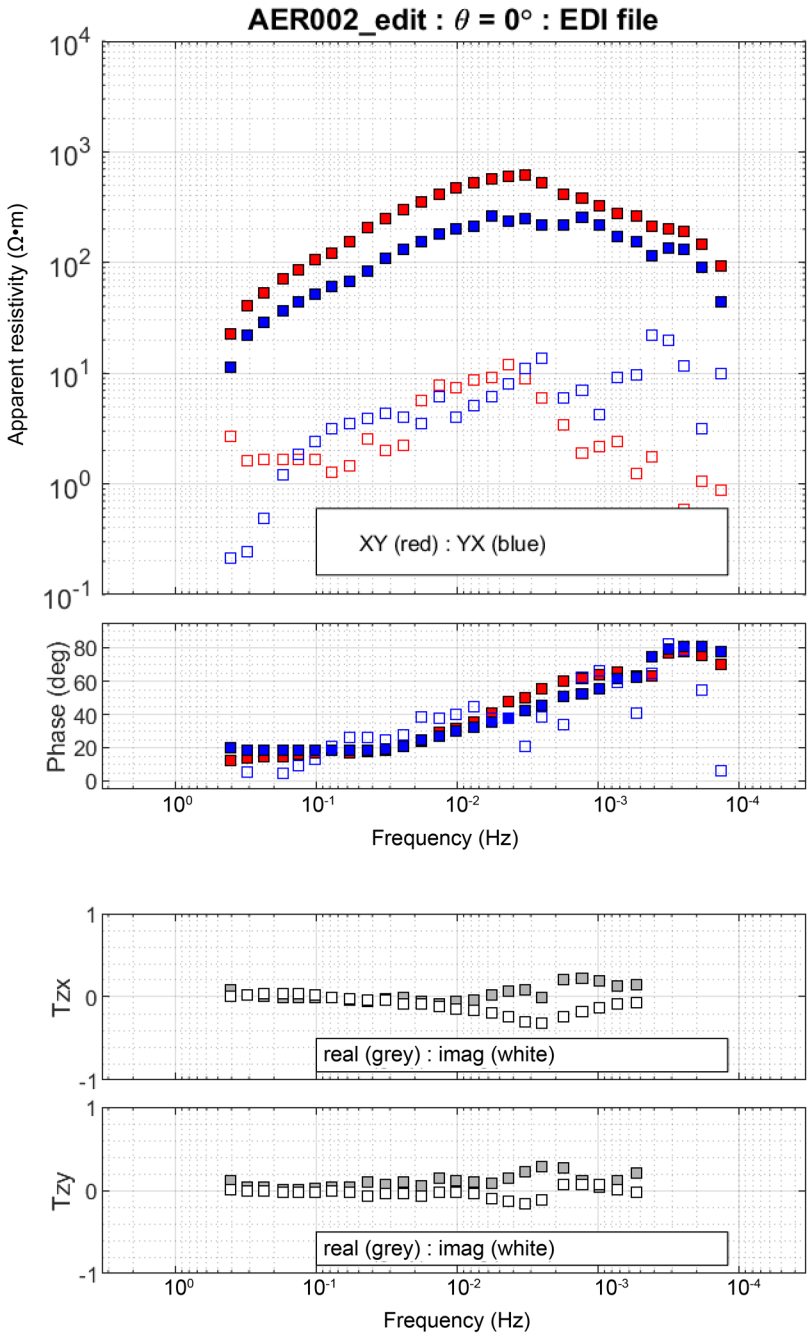

Figure 15. Data from station AER 002 (lat. 56.96°N, long. 113.60°W). In the top two panels, the solid red boxes are the XY component of the impedance tensor, solid blue boxes are the YX component, open red boxes are the XX component, and open blue boxes are the YY component. In the bottom two panels, the grey and white boxes are the real (in-phase) and the imaginary (imag; out-of-phase) components of the tipper (T), respectively. Abbreviations: Ω, ohms; deg, degrees.

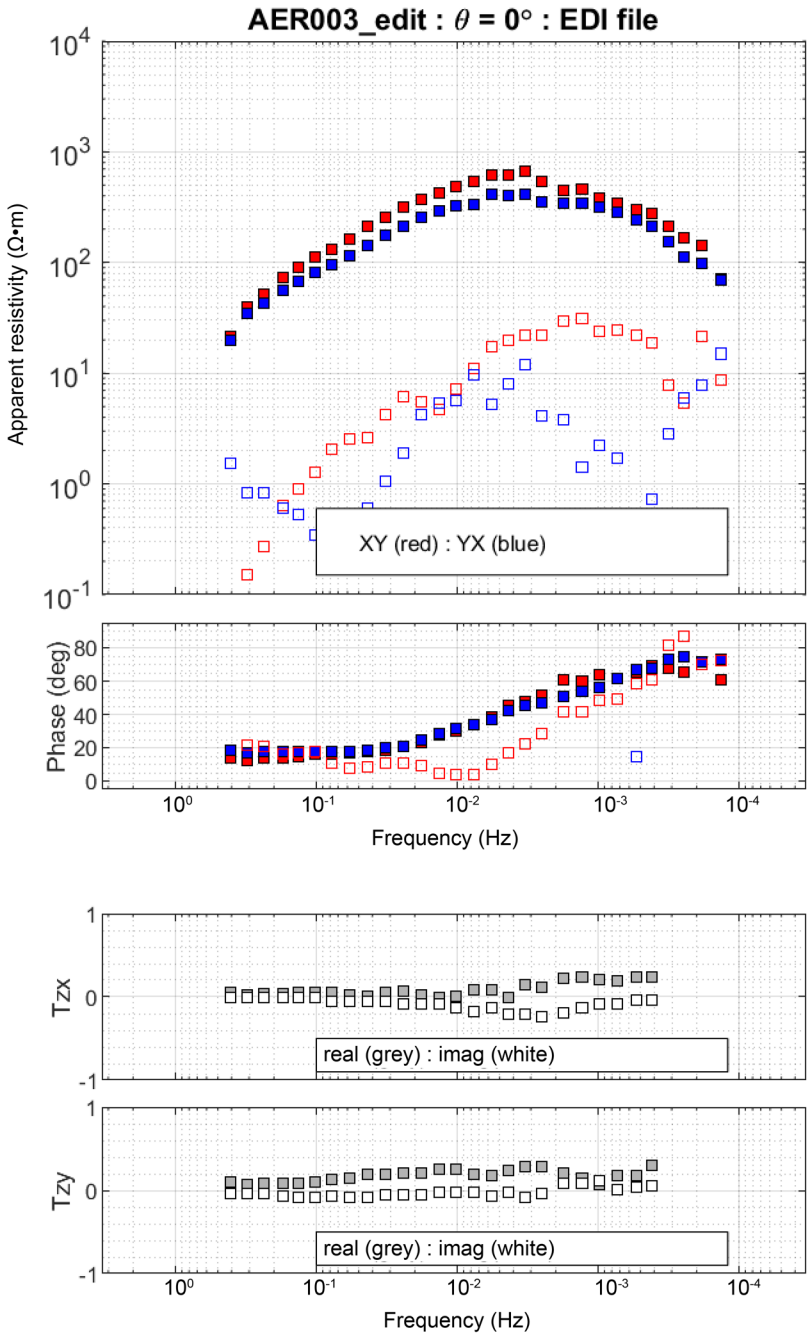

Figure 16. Data from station AER 003 (lat. 56.63°N, long. 113.53°W). In the top two panels, the solid red boxes are the XY component of the impedance tensor, solid blue boxes are the YX component, open red boxes are the XX component, and open blue boxes are the YY component. In the bottom two panels, the grey and white boxes are the real (in-phase) and the imaginary (imag; out-of-phase) components of the tipper (T), respectively. Abbreviations: Ω, ohms; deg, degrees.

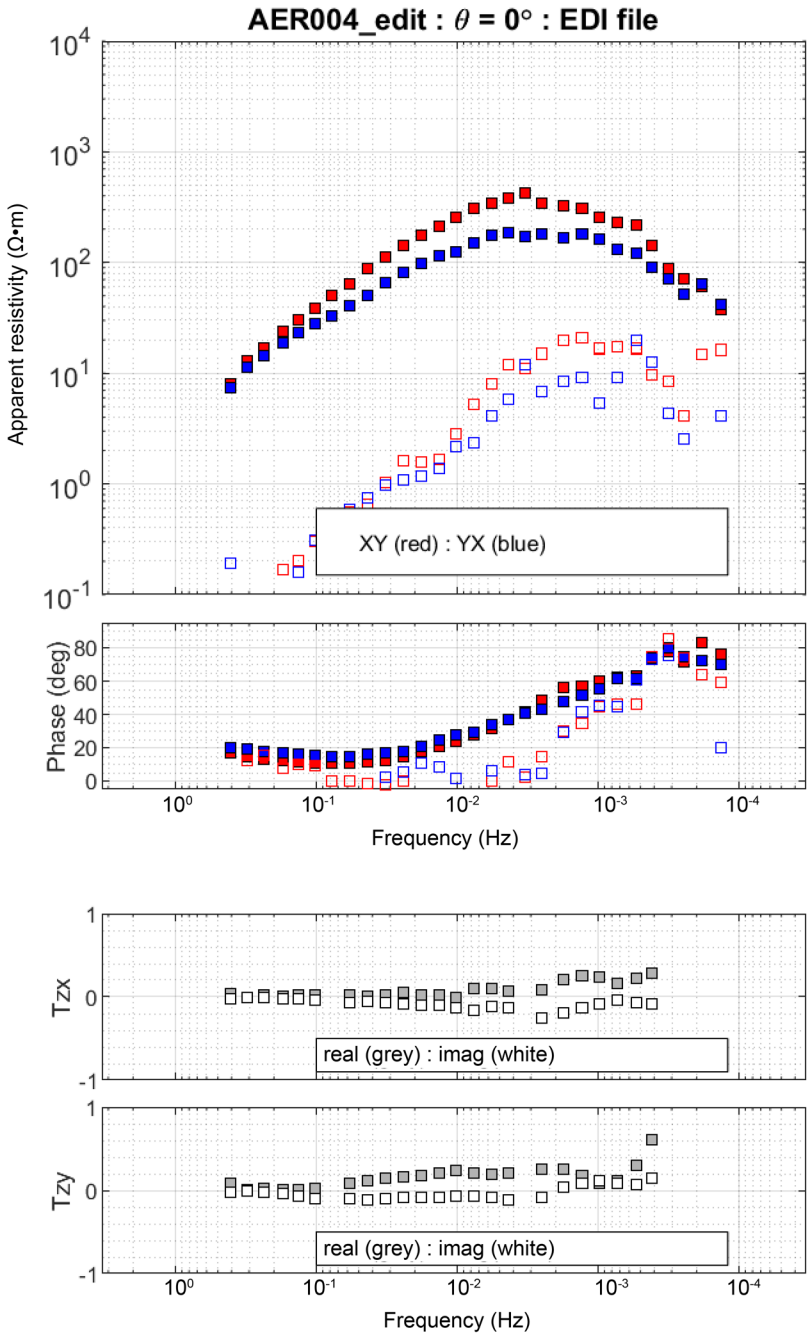

Figure 17. Data from station AER 004 (lat. 56.65°N, long. 114.03°W). In the top two panels, the solid red boxes are the XY component of the impedance tensor, solid blue boxes are the YX component, open red boxes are the XX component, and open blue boxes are the YY component. In the bottom two panels, the grey and white boxes are the real (in-phase) and the imaginary (imag; out-of-phase) components of the tipper (T), respectively. Abbreviations: Ω, ohms; deg, degrees.

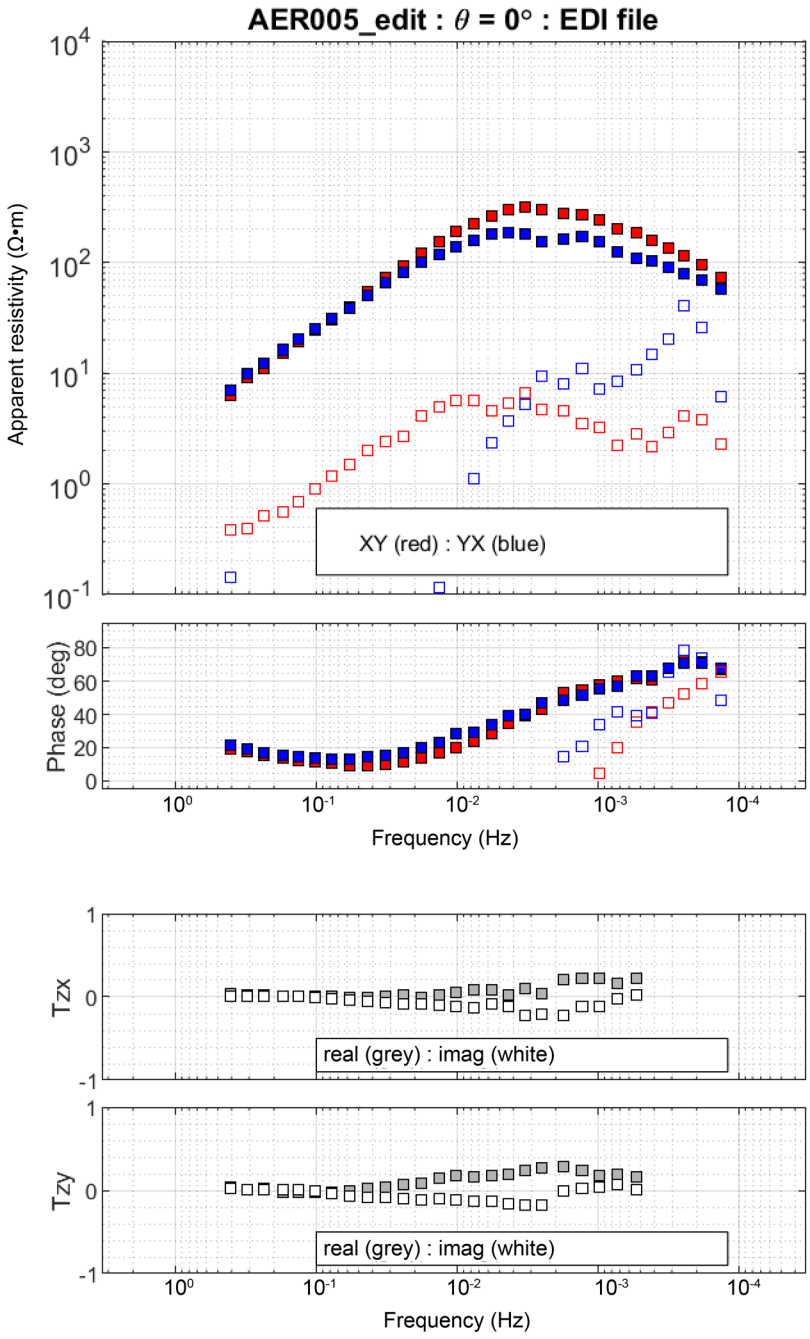

Figure 18. Data from station AER 005 (lat. 56.36°N, long. 114.46°W). In the top two panels, the solid red boxes are the XY component of the impedance tensor, solid blue boxes are the YX component, open red boxes are the XX component, and open blue boxes are the YY component. In the bottom two panels, the grey and white boxes are the real (in-phase) and the imaginary (imag; out-of-phase) components of the tipper (T), respectively. Abbreviations: Ω, ohms; deg, degrees.

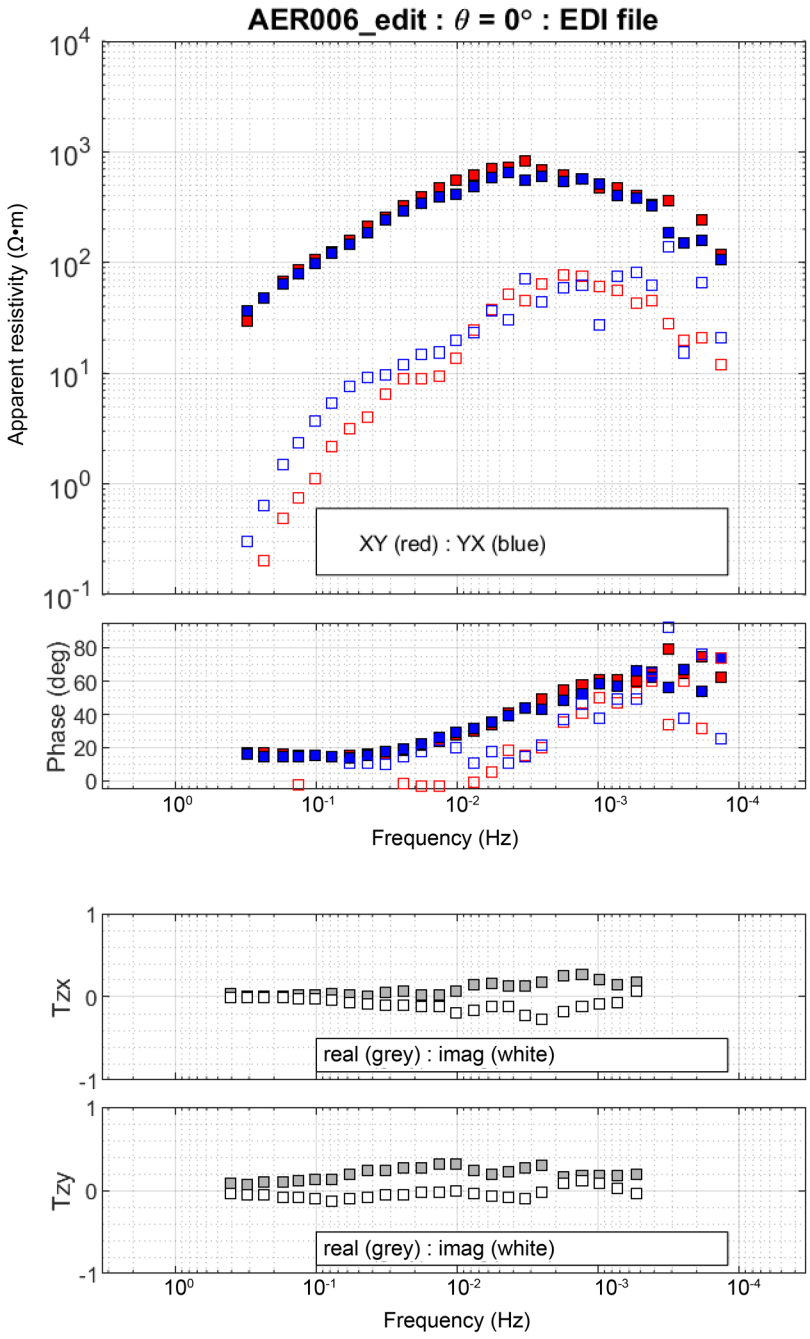

Figure 19. Data from station AER 006 (lat. 56.37°N, long. 113.66°W). In the top two panels, the solid red boxes are the XY component of the impedance tensor, solid blue boxes are the YX component, open red boxes are the XX component, and open blue boxes are the YY component. In the bottom two panels, the grey and white boxes are the real (in-phase) and the imaginary (imag; out-of-phase) components of the tipper (T), respectively. Abbreviations: Ω, ohms; deg, degrees.

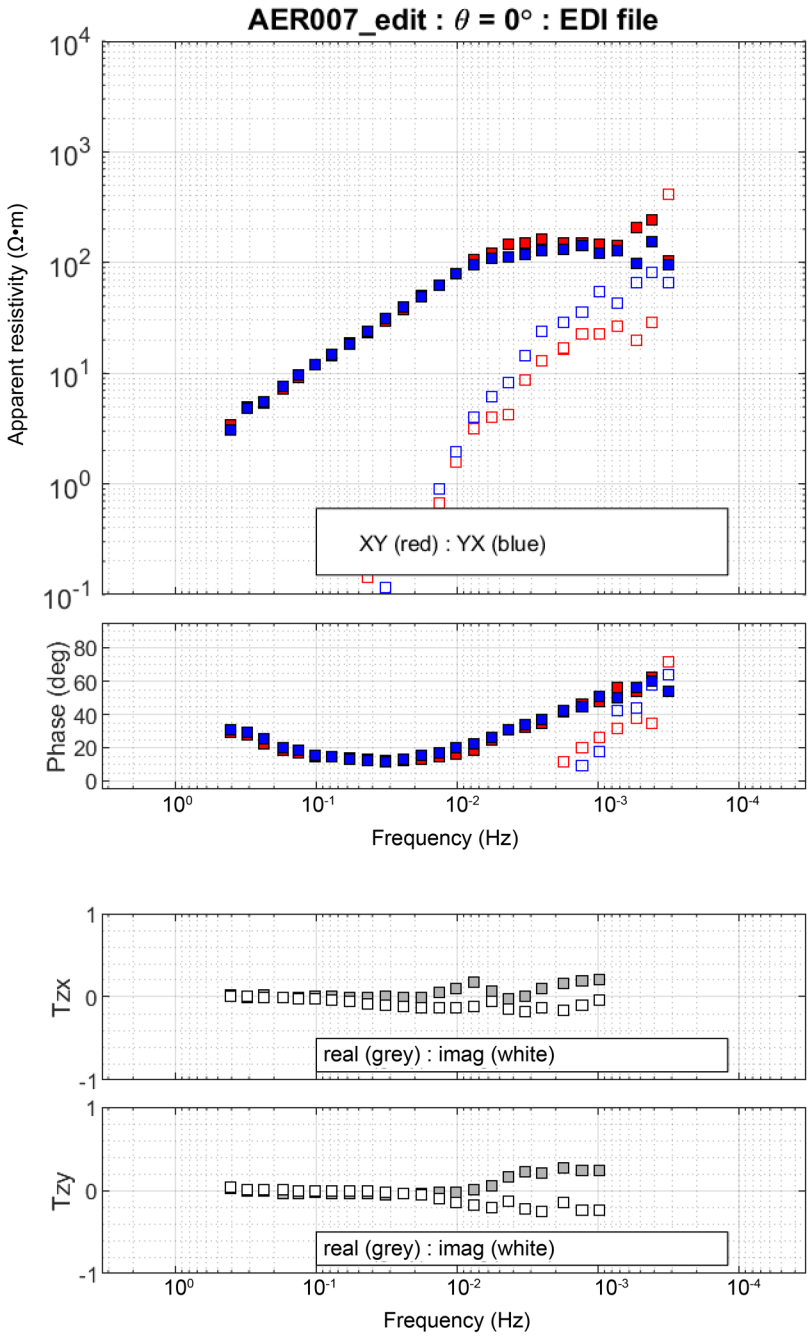

Figure 20. Data from station AER 007 (lat. 55.78°N, long. 115.95°W). In the top two panels, the solid red boxes are the XY component of the impedance tensor, solid blue boxes are the YX component, open red boxes are the XX component, and open blue boxes are the YY component. In the bottom two panels, the grey and white boxes are the real (in-phase) and the imaginary (imag; out-of-phase) components of the tipper (T), respectively. Abbreviations: Ω, ohms; deg, degrees.

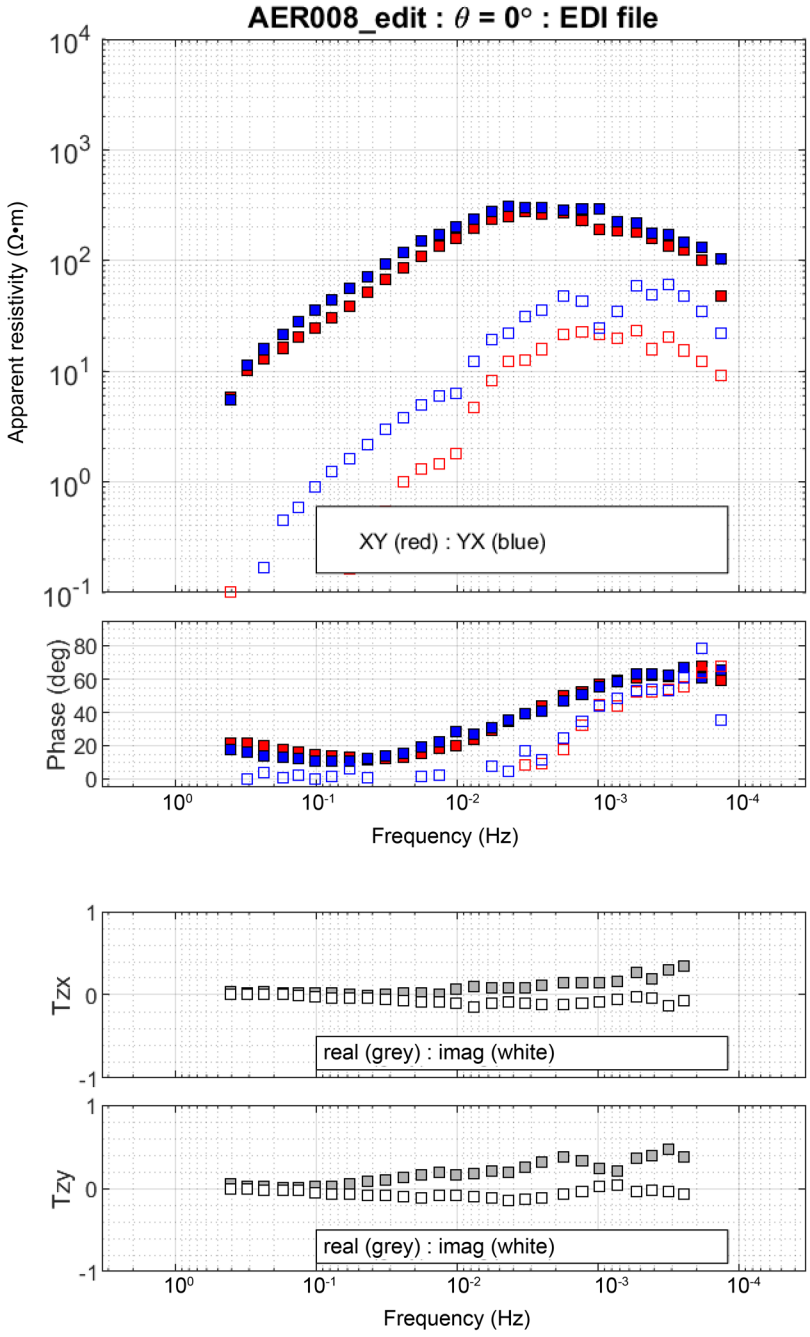

Figure 21. Data from station AER 008 (lat. 56.76°N, long. 114.63°W). In the top two panels, the solid red boxes are the XY component of the impedance tensor, solid blue boxes are the YX component, open red boxes are the XX component, and open blue boxes are the YY component. In the bottom two panels, the grey and white boxes are the real (in-phase) and the imaginary (imag; out-of-phase) components of the tipper (T), respectively. Abbreviations: Ω, ohms; deg, degrees.

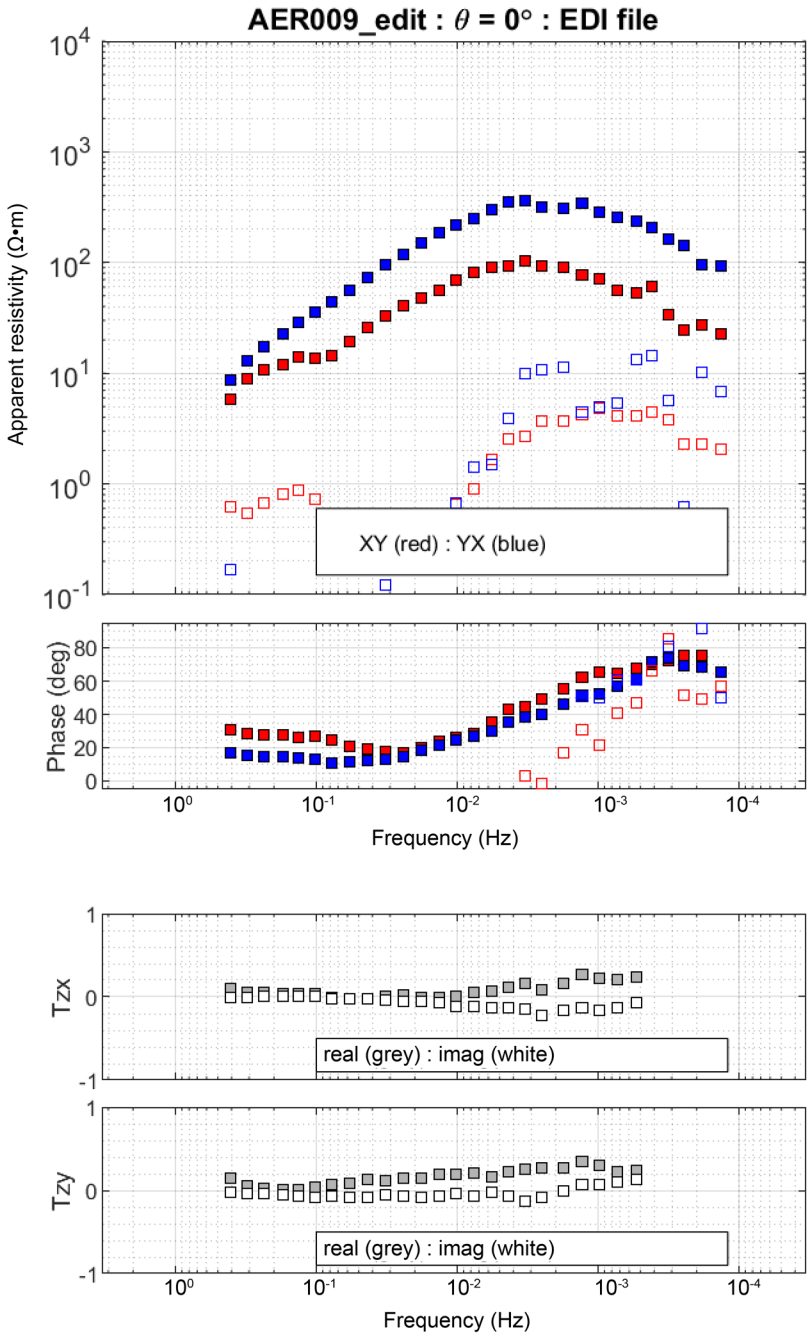

Figure 22. Data from station AER 009 (lat. 57.19°N, long. 114.46°W). In the top two panels, the solid red boxes are the XY component of the impedance tensor, solid blue boxes are the YX component, open red boxes are the XX component, and open blue boxes are the YY component. In the bottom two panels, the grey and white boxes are the real (in-phase) and the imaginary (imag; out-of-phase) components of the tipper (T), respectively. Abbreviations: Ω, ohms; deg, degrees.

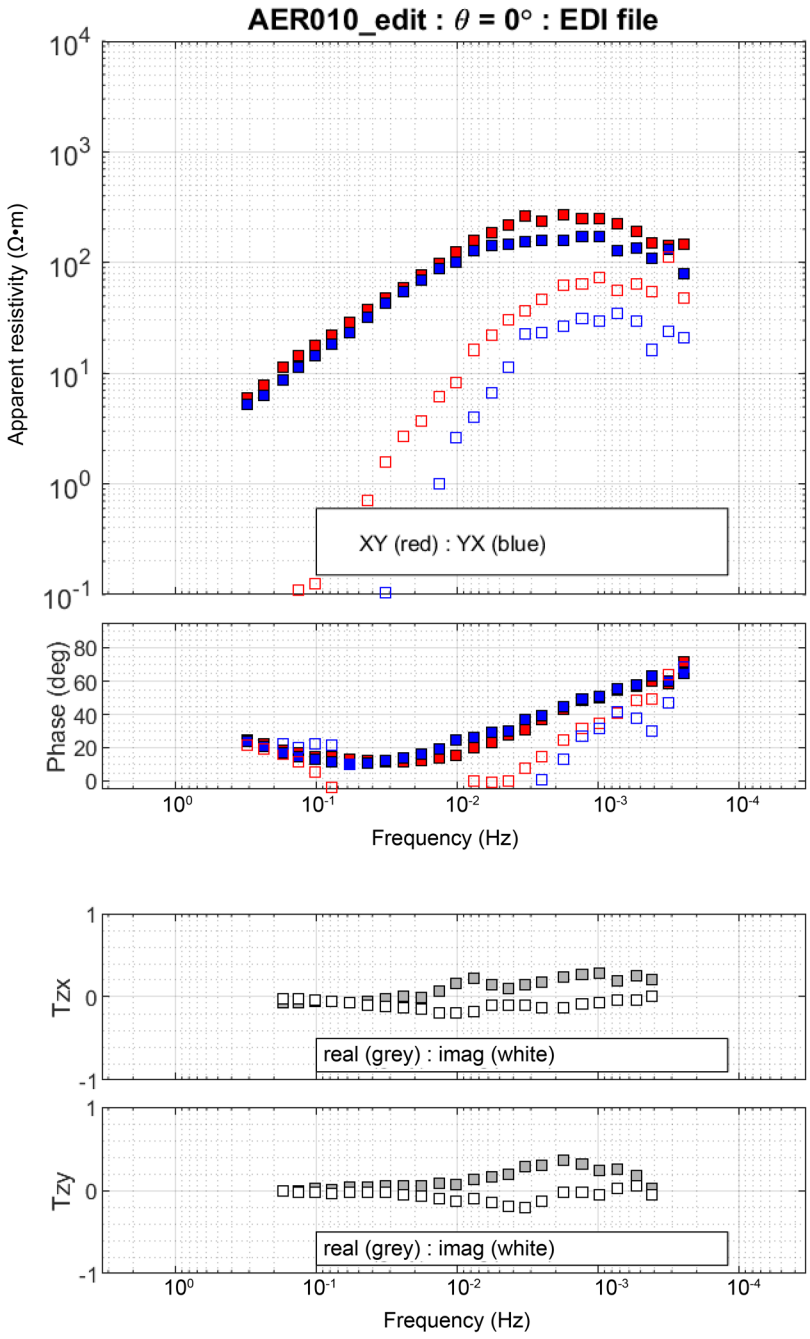

Figure 23. Data from station AER 010 (lat. 56.15°N, long. 115.93°W). In the top two panels, the solid red boxes are the XY component of the impedance tensor, solid blue boxes are the YX component, open red boxes are the XX component, and open blue boxes are the YY component. In the bottom two panels, the grey and white boxes are the real (in-phase) and the imaginary (imag; out-of-phase) components of the tipper (T), respectively. Abbreviations: Ω, ohms; deg, degrees.

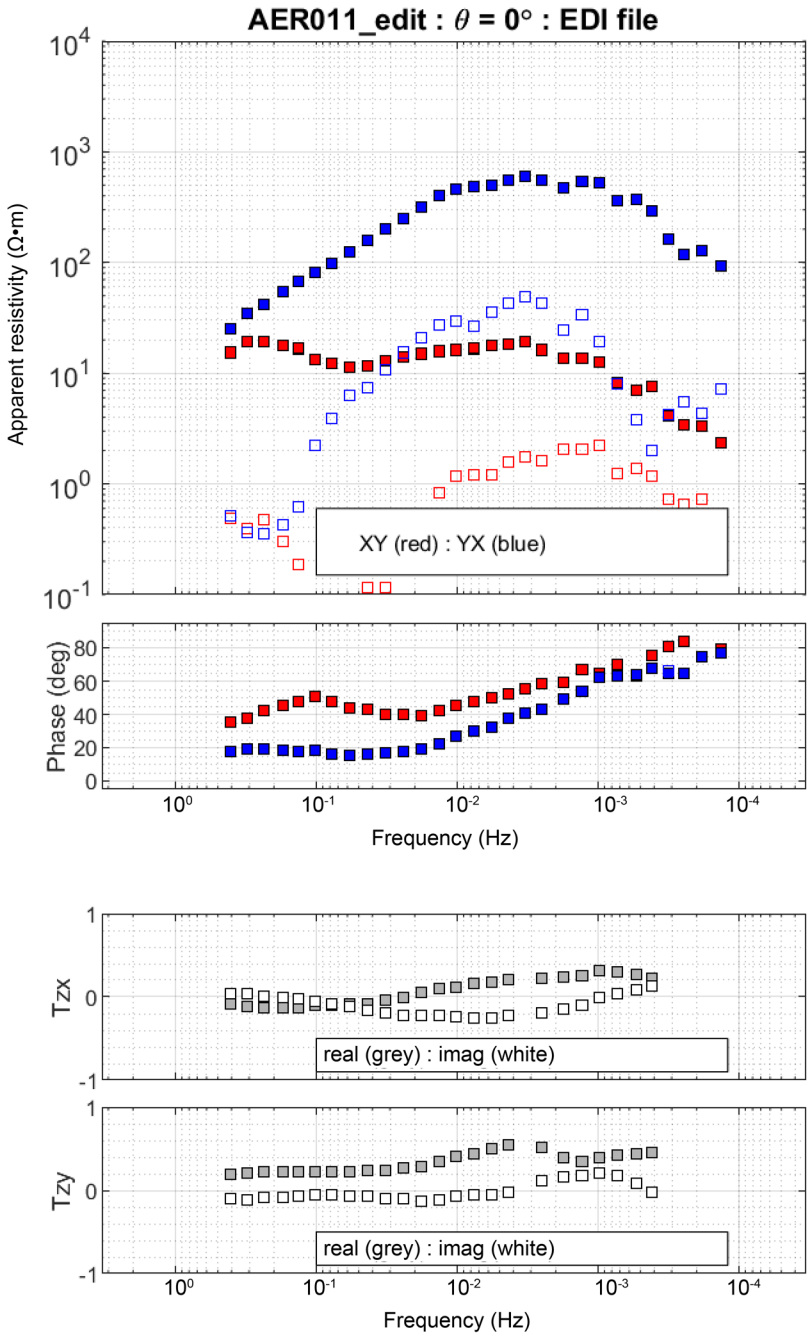

Figure 24. Data from station AER 011 (lat. 57.57°N, long. 111.93°W). In the top two panels, the solid red boxes are the XY component of the impedance tensor, solid blue boxes are the YX component, open red boxes are the XX component, and open blue boxes are the YY component. In the bottom two panels, the grey and white boxes are the real (in-phase) and the imaginary (imag; out-of-phase) components of the tipper (T), respectively. Abbreviations: Ω, ohms; deg, degrees.

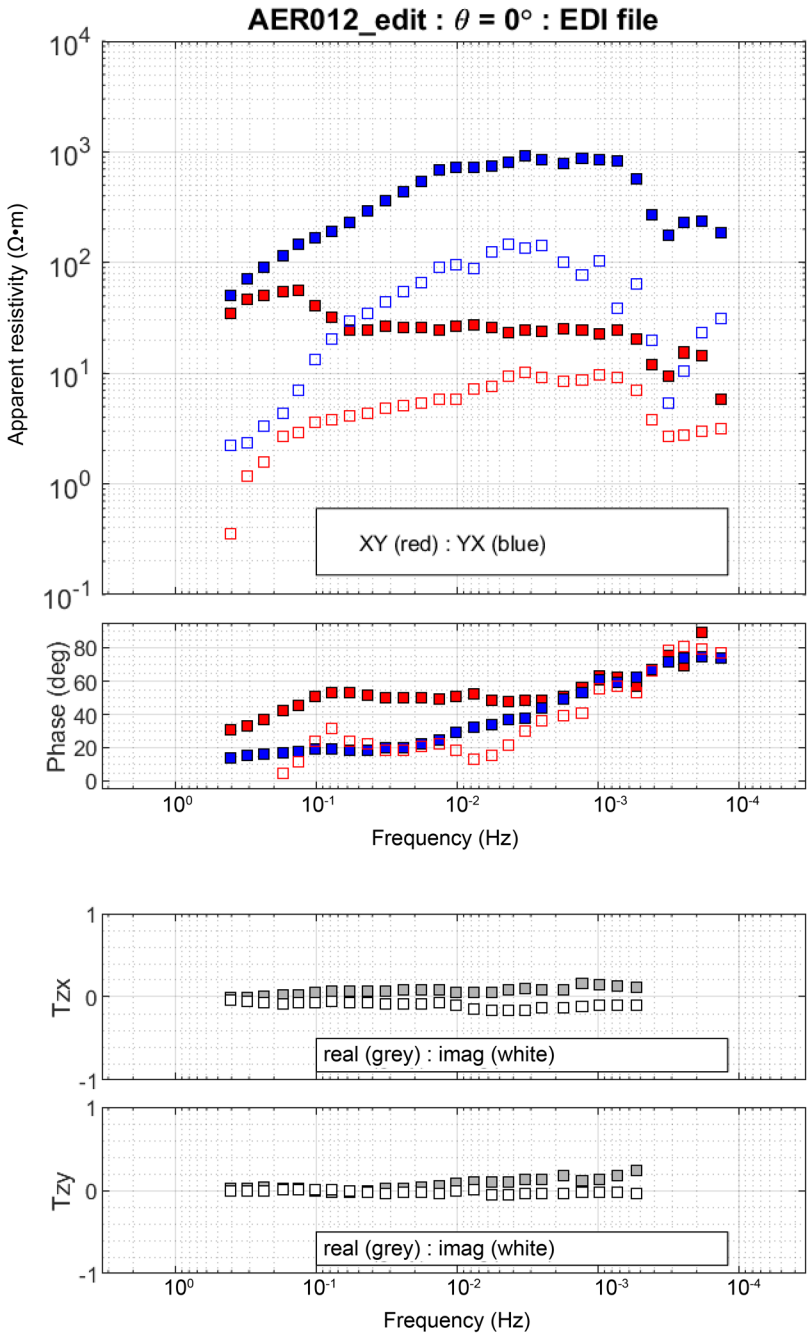

Figure 25. Data from station AER 012 (lat. 57.88°N, long. 112.42°W). In the top two panels, the solid red boxes are the XY component of the impedance tensor, solid blue boxes are the YX component, open red boxes are the XX component, and open blue boxes are the YY component. In the bottom two panels, the grey and white boxes are the real (in-phase) and the imaginary (imag; out-of-phase) components of the tipper (T), respectively. Abbreviations: Ω, ohms; deg, degrees.

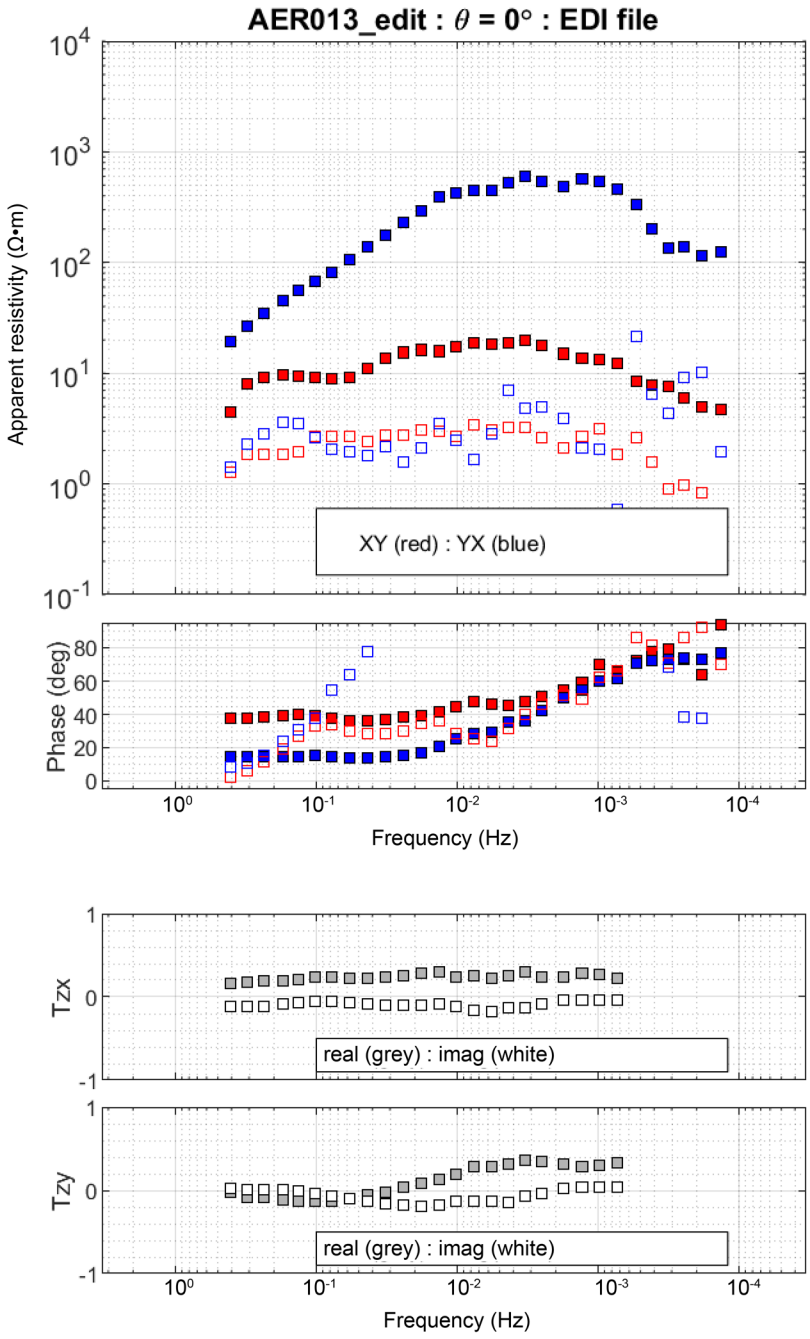

Figure 26. Data from station AER 013 (lat. 57.79°N, long. 111.94°W). In the top two panels, the solid red boxes are the XY component of the impedance tensor, solid blue boxes are the YX component, open red boxes are the XX component, and open blue boxes are the YY component. In the bottom two panels, the grey and white boxes are the real (in-phase) and the imaginary (imag; out-of-phase) components of the tipper (T), respectively. Abbreviations: Ω, ohms; deg, degrees.

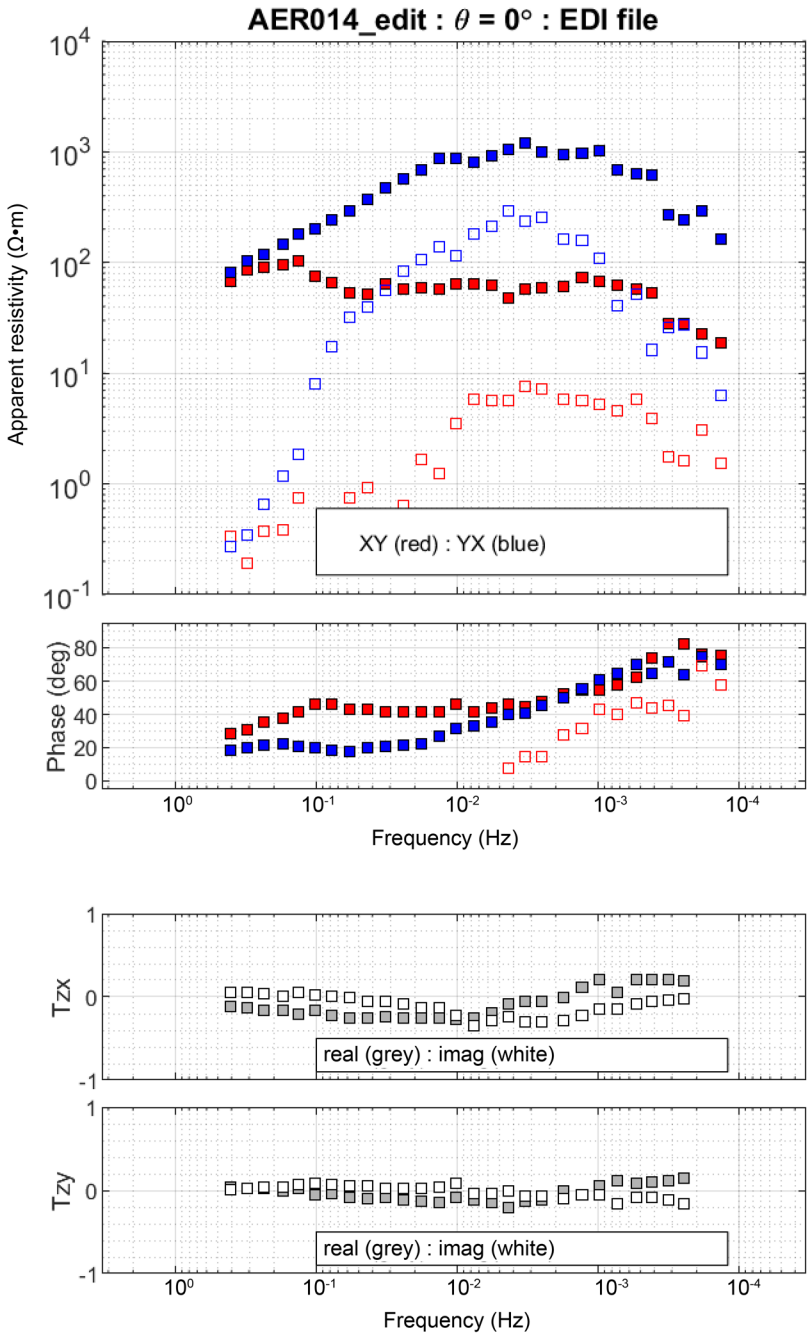

Figure 27. Data from station AER 014 (lat. 57.29°N, long. 112.30°W). In the top two panels, the solid red boxes are the XY component of the impedance tensor, solid blue boxes are the YX component, open red boxes are the XX component, and open blue boxes are the YY component. In the bottom two panels, the grey and white boxes are the real (in-phase) and the imaginary (imag; out-of-phase) components of the tipper (T), respectively. Abbreviations: Ω, ohms; deg, degrees.

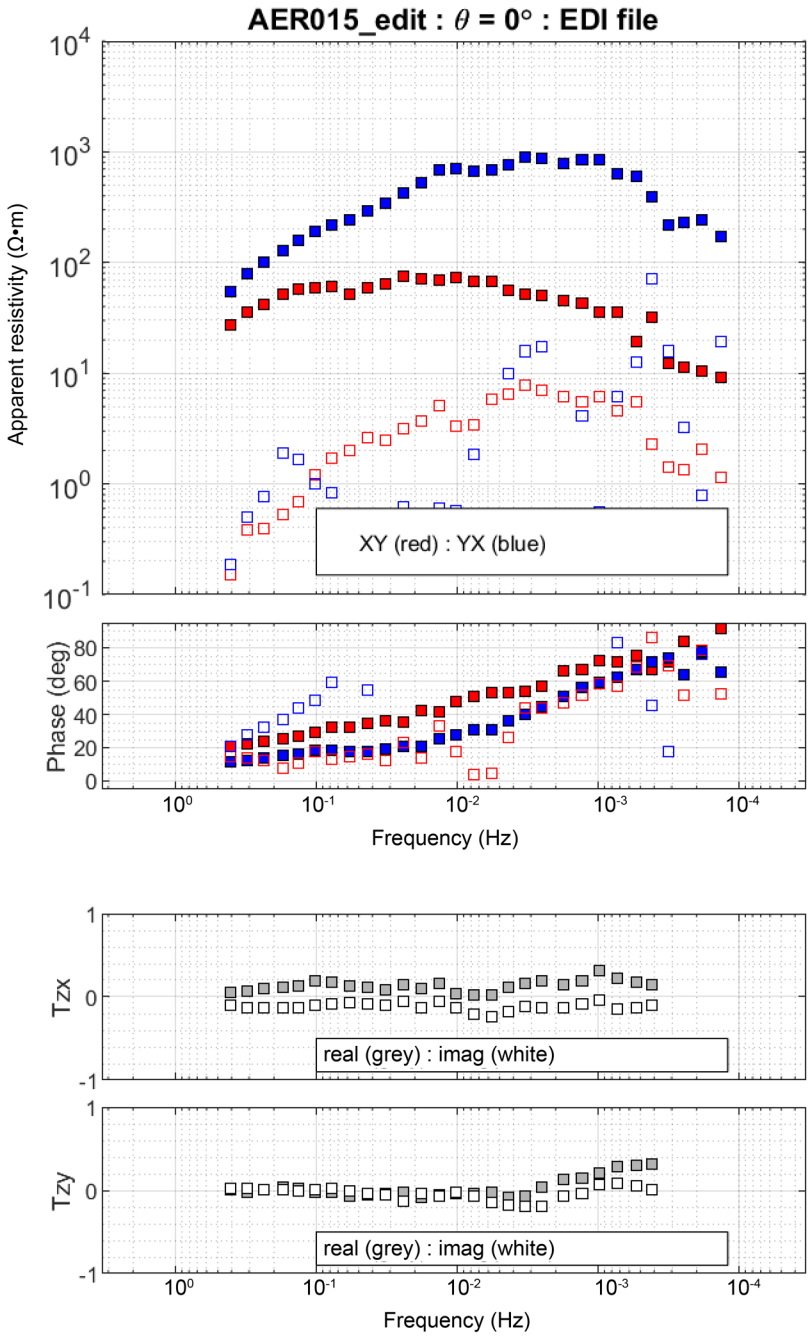

Figure 28. Data from station AER 015 (lat. 57.87°N, long. 113.48°W). In the top two panels, the solid red boxes are the XY component of the impedance tensor, solid blue boxes are the YX component, open red boxes are the XX component, and open blue boxes are the YY component. In the bottom two panels, the grey and white boxes are the real (in-phase) and the imaginary (imag; out-of-phase) components of the tipper (T), respectively. Abbreviations: Ω, ohms; deg, degrees.